Diversity of visual inputs to Kenyon cells of the *Drosophila* mushroom body

Ishani Ganguly[1,3*], Emily L. Heckman[2*], Ashok Litwin-Kumar[1,3], E. Josephine Clowney[2,4#], Rudy Behnia[1#]

*These authors contributed equally to this work. Authorship order was determined by coin toss.

#These authors contributed equally to this work and are both corresponding authors.

1. The Mortimer B. Zuckerman Mind Brain Behavior Institute, Department of Neuroscience, Columbia University, New York, NY 10027, USA
2. Department of Molecular, Cellular, and Developmental Biology, University of Michigan, Ann Arbor, MI 48109, USA
3. Center for Theoretical Neuroscience, Columbia University, New York, NY 10027, USA
4. Michigan Neuroscience Institute Affiliate

Abstract

The arthropod mushroom body is well-studied as an expansion layer that represents olfactory stimuli and links them to contingent events. However, 8% of mushroom body Kenyon cells in *Drosophila melanogaster* receive predominantly visual input, and their tuning and function are poorly understood. Here, we use the FlyWire adult whole-brain connectome to identify inputs to visual Kenyon cells. The types of visual neurons we identify are similar across hemispheres and connectomes with certain inputs highly overrepresented. Many visual projection neurons presynaptic to Kenyon cells receive input from large swathes of visual space, while local visual interneurons, providing smaller fractions of input, receive more spatially restricted signals that may be tuned to specific features of the visual scene. Like olfactory Kenyon cells, visual Kenyon cells receive sparse inputs from different combinations of visual channels, including inputs from multiple optic lobe neuropils. The sets of inputs to individual visual Kenyon cells are consistent with random sampling of available inputs. These connectivity patterns suggest that visual coding in the mushroom body, like olfactory coding, is sparse, distributed, and combinatorial. However, the expansion coding properties appear different, with a specific repertoire of visual inputs projecting onto a relatively small number of visual Kenyon cells.

Introduction

In expansion layers, large populations of neurons with shared or similar developmental identity receive inputs from neurons carrying diverse sensory signals. Prominent examples include the lophotrochozoan parallel lobe system and chordate cerebellum, hippocampus, pallium, and cortex. A well-studied example is the mushroom body of *Drosophila melanogaster*, where ~2000 intrinsic neurons, called Kenyon cells, link sensory representations to proximate events via dopamine-mediated synaptic plasticity[1–6]. The mushroom body is thought to have evolved as an olfactory structure, and in *Drosophila*, more than 90% of Kenyon cells receive predominantly olfactory input[7–9]. However, 8% of Kenyon cells in *Drosophila* receive mainly visual inputs, and radical expansions of the visual mushroom body have occurred independently in several arthropod clades[7,9].

Flies have two subsets of visual Kenyon cells. KCγ-d cells (KCγ-d's) are the first Kenyon cells to be generated in development[10–12]. They receive olfactory input in the larval mushroom body, but re-wire during metamorphosis to innervate the ventral accessory calyx (vACA)[7,10,13,14]. In the adult, they have been shown to receive direct input from the medulla through the VPN-MB1 and VPN-MB2 visual projection neurons[15] and the accessory medulla through aMe12[7,16]. KCαβ-p cells (KCαβ-p's) are born during pupal stages, before olfactory αβ cells, and innervate the dorsal accessory calyx (dACA)[10]. They have been shown to receive indirect visual input through local visual interneurons (LVINs) processing signals from the lobula[17,18]. These experimental observations were augmented by a description of the repertoire of visual interneurons providing inputs to the mushroom body in the hemibrain connectome dataset, which highlighted the previously unexpected extent of visual projections to this area[7].

The visual system of the fruit fly is composed of four main neuropils: the lamina, the medulla, the lobula and the lobula plate. The accessory medulla is a lesser known small optic lobe neuropil, tucked between the medulla and the lobula, where the extraocular photoreceptors of the Hofbauer–Buchner "eyelet" send their axons. aMe neurons receive direct input from retinal photoreceptor cells as well as from eyelet photoreceptors[16,19]. Clock neurons also innervate the accessory medulla[20–23]. The role of the accessory medulla has not been investigated in *Drosophila,* but in other insect species it has been implicated in entrainment of the circadian clock[24]. While analyses of the hemibrain connectome were able to identify visual interneurons providing input to the mushroom body and found that visual projection neurons (VPNs) from the medulla, lobula and aMe innervate the calyx, the identity of these VPNs could not be determined due to the lack of comprehensive reconstruction of the optic lobe neuropils[7,25].

In adult *Drosophila melanogaster*, olfactory Kenyon cells have between 3 and 10 large, claw-shaped dendrites that each receive input from a single, multisynaptic "bouton" deriving from cholinergic olfactory projection neurons in the antennal lobe[26–31]. Individual Kenyon cells only spike when multiple of their inputs are active. They thus form a sparse, combinatorial code for chemical features of odor space that improves stimulus discriminability as compared to the antennal lobe representation[32–34]. In contrast to the well-studied olfactory representation, it is still unclear what kind of visual information is conveyed to the MB, how visual information is encoded in Kenyon cells, and what this information is used for. Whereas blue versus green color learning[1,15,35,36] and context generalization[37] have been shown to specifically require the mushroom body, multiple visual learning paradigms, such as place learning[38] and pattern recognition[39,40], have been shown to rely on the central complex (CX). In terms of multisensory learning, which has been established in the context of memory enhancement[41,42] and transfer between olfaction and vision[41], the association between olfactory and visual information has been suggested to rely on the mushroom body[43]. The mushroom body has been shown to be required for learning of color associations in honeybees, learning of spatial associations in cockroaches, and navigation in ants[44–46].

Here, we use the FlyWire adult whole brain electron microscopy connectome to describe the repertoires of inputs to individual visual Kenyon cells in *Drosophila melanogaster*[8,47,48]. Consistent with previous reports, direct VPNs dominate input to KCγ-d cells, while indirect visual input via LVINs dominates input to KCαβ-p cells[7,15,17]. We focus our analysis on KCγ-d's and find that individual Kenyon cells can receive inputs from mixtures of

presynaptic partners, including from both VPNs and LVINs and from multiple optic lobe neuropils. Many KC-projecting VPNs receive input from large swathes of visual space, while some KC-projecting LVINs receive more spatially restricted signals across visual space, a wiring logic that would provide Kenyon cells with both information about full-field conditions of the environment and translational invariance for a limited number of specific visual features. Previous work found that aMe12 accessory medulla neurons provide input to visual Kenyon cells, and we find that inputs from this small neuropil are prominent overall[7,16], providing a potential link between the circadian system and the MB. We find that like olfactory Kenyon cells, visual Kenyon cells receive sparse inputs, from 1-7 neurons each. Finally, we compare the input patterns to individual Kenyon cells between hemispheres and to a random model; input patterns vary across hemispheres in this brain and are consistent with a random sampling of available inputs, but certain inputs are highly overrepresented compared to others in both hemispheres. These connectivity patterns suggest that on the one hand, visual coding in the mushroom body, like olfactory coding, is sparse, distributed, and combinatorial. On the other hand, the expansion coding properties appear different, as a specific repertoire of visual input types project onto a relatively small number of visual Kenyon cells.

Results

Visual projection neurons dominate input to the ventral accessory calyx, and local visual interneurons to the dorsal accessory calyx

Sensory information is conveyed to the dendrites of Kenyon cells in the mushroom body calyces. The main calyx contains the dendrites of olfactory Kenyon cells, representing 90% of the total population. Previous connectomics analyses in the hemibrain dataset revealed that other sensory streams make connections in accessory calyces[7]. Visual inputs segregate into two streams of information that target KCγ-d cells (KCγ-d's) in the ventral accessory calyx and KCαβ-p cells (KCαβ-p's) in the dorsal accessory calyx (Figure 1A, B). Each population receives both direct and indirect inputs (through LVINs) from VPNs (Figure 1A). In the hemibrain dataset, the proportion of direct vs. indirect inputs was shown to be different in the two accessory calyces: The ventral pathway is enriched in direct VPNs whereas the dorsal pathway is enriched in indirect connections[7].

In the FlyWire reconstruction, we observe 147 and 148 KCγ-d cells on the left and right respectively; and 67 versus 61 KCαβ-p's. As in the hemibrain dataset, VPNs make up the majority of visual input onto KCγ-d's (49 of 74 presynaptic partners, 75% of input synapses), while LVINs constitute about a third of the inputs (Figure 1C, D; Supplemental Table 1). Another prominent input to the KCγ-d population is the large inhibitory neuron APL, which makes on average 16 and 10 synapses per KCγ-d in the left and right hemispheres respectively (comparable to the average number of synapses APL makes onto each KCγ-m). In contrast to a previous observation that KCγ-d's do not have clawed dendrites[7], we observe KCγ-d's that make bouton-claw and *en passant* synapses with incoming VPNs and LVINs (Figure 1 Supplement 1).

For KCαβ-p's, LVINs dominate the information flow (62.5% of presynaptic partners/84% of synapses) (Figure 1F, G; Supplemental Table 2). Few inputs are shared between KCγ-d's and KCαβ-p's (Figure 1I). A ranking of

VPNs and LVINs in terms of total synapse numbers made onto KCγ-d's shows that while VPNs are the main inputs, several LVINs are among the highest connected neurons (Figure 1E). In the dorsal pathway to KCαβ-p's, LVINs constitute the bulk of the inputs but several VPNs are intermingled among them (Figure 1H). As LVINs are potential nodes for multisensory integration, receiving not only visual information through indirect VPNs but also information from other sensory modalities[7], the dorsal and ventral pathways likely contribute differently to visual vs. multimodal mushroom body functions. While we expect the indirect and potentially multimodal inputs to KCαβ-p's will be very interesting for future study, we elected here to focus subsequent analyses on the more numerous KCγ-d's, as their receipt of strong, direct VPN inputs allows us to infer their visual tuning.

Direct visual inputs to the ventral accessory calyx derive from all optic lobe neuropils

We identified 49 VPNs that form connections of at least 5 synapses onto KCγ-d's in the left hemisphere of the FlyWire dataset. 18 of these derive from the medulla (44% of synapses), 18 from the lobula (26.4% of synapses) and 13 from the accessory medulla (29.5% of synapses) (Figure 2A-C). Like olfactory projection neurons, all direct VPNs are predicted to be cholinergic, and therefore excitatory. None of the VPNs connecting to the vACA have assigned functions. In order to classify them further, we used both anatomy and connectivity to cluster these VPNs into putative cell types (Figure 2D, see Methods). Among the 18 medulla VPNs, most are singlets: They do not cluster with any other MB-projecting visual neurons and appear only once in each hemisphere. The one exception is a cluster comprising three neurons (ME.PLP.36, ME.PLP.42 and ME.1557). Like medulla VPNs, most of the 18 lobula VPNs are singlets, though LO.SCL.7 and LO.SLP.12 form a cluster. In contrast, aMe VPNs providing input to the left vACA can be classified into just four cell types, aMe12, aMe20 or aMe26_L and aMe26_R. There are 4 aMe12s on each side of the brain, and KCγ-d's contact all 8 individual neurons (7 with more than 5 synapses, 1 with fewer). KCγ-d's contact 5/6 aMe26 neurons in the brain. There is only one aMe20 in each hemisphere. Therefore, KCγ-d's contact most individual members of these cell types. aMe12 neurons receive direct input from photoreceptor cells[16], and thus their inputs to Kenyon cells are of the same circuit depth as olfactory projection neurons inputs, i.e. two synapses from the periphery. Most other paths to KCγ-d's appear to be three or more synapses from the periphery.

Generally, there is a clear absence of retinotopic columnar cell types among VPNs contacting the vACA. They are all large field neurons and many of them have dendrites restricted to the ventral part of the medulla. All medulla and lobula neurons are ipsilaterally connected. aMe12 and aMe26_R are the only direct VPNs connected both ipsi- and contralaterally. The top types of VPNs from each neuropil dominate synaptic input to KCγ-d's overall (Figure 2E). As we will describe further below, these types dominate mushroom body inputs more prominently than do top olfactory types. We ranked VPN types by the sum of synapses they make onto KCγ-d's (Figure 2F). Neurons from all three visual neuropils are among the top 5 input types, suggesting that signals from each neuropil are likely to have a strong influence on KCγ-d activity. The strongest connected neurons also are the ones that contact the most Kenyon cells (Figure 2F, G).

As can be seen in the neuronal skeletons in Figure 2D, every VPN innervating the mushroom body calyx also projects to other regions of the brain. Their processes in the central brain make a large number of connections

with other nearby regions such as the PLP or SLP, indicating that the signals they carry are used not only in the mushroom body in the context of learning and memory but also in other brain areas for other purposes. Similarly, uniglomerular olfactory projections that provide input to the mushroom body extend a second axonal branch to the lateral horn where they regulate innate behaviors[26,49].

LVIN inputs to the ventral accessory calyx provide structured visual inputs

In addition to direct VPNs, KCγ-d's also receive visual inputs indirectly through LVINs (Figure 1A, C). These are central brain interneurons with no arborizations in the optic lobe but that themselves receive inputs from VPNs[7]. We have identified 25 LVINs in the left hemisphere of the FlyWire reconstruction that make 5 or more synapses with KCγ-d's, corresponding to 21 cell types (Figure 1E, 3A). The highest connected LVIN, PLP095 (PLP.78 in Flywire), makes 438 synapses with a total of 24 KCγ-d's, while the median LVIN makes 11 synapses across 2 KCγ-d's. 19 of the LVINs are predicted to be cholinergic (i.e. excitatory) while 5 are predicted to be GABA/glutamatergic (inhibitory) (Figure 3C). These neurons also receive diverse inputs from other central brain neurons, including multiglomerular PNs, making these potential nodes of multisensory integration (Figure 3 Supplement 2C).

Each LVIN gets inputs from multiple VPNs and the same VPN can make connections with multiple LVINs (Figure 3F). We have identified 226 "indirect" VPN inputs that make 5 or more synapses with KCγ-d-connected LVINs (Figure 3A, F). A striking finding is that among them, we find repeated 36 out of the 49 direct VPNs described in Figure 2 (Figure 3B). In particular, all three direct aMe types connect with KCγ-d's both directly and indirectly through LVINs (Figure 3F). Additional aMe neurons (aMe3, aMe5, aMe19a and aMe25) are included in the indirect pathway. A small number of lobula plate neurons and ocellar neurons also provide inputs to LVINs. Despite not being represented in the direct VPN class, several types of small-field neurons whose dendrites tile the extent of the medulla/lobula, such as lobula columnar neurons (LCs) or medulla columnar neurons (MCs), provide inputs to LVINs contacting KCγ-d's (Figure 3F, Figure3 Supplement 1A). When only inspecting neurons that make ≥5 synapses, we noticed that not all members of an LC or MC cell type are connected to an LVIN, giving rise to a seemingly random salt and pepper organization of receptive fields (Figure 3 Supplement 1B, C). However when removing the synapse threshold, 49 out of 52 LC15, for instance, are connected to KCγ-d-projecting LVINs, encompassing the extent of the lobula (Figure 3 Supplement 1B, D). This is also true of LC24 where 53/62 neurons are connected (Figure 3 Supplement 1C, D). In the case of MC62, although removing the threshold does include additional neurons, they are all restricted to the ventral half of the medulla, leaving out the MC62s that occupy the dorsal half (Figure 3 Supplement 1E-G).

The connectivity matrix of VPN inputs onto vACA-projecting LVINs (Figure 3E) highlights interesting properties. The connectivity appears highly structured; certain VPN cell types make connections with few and particular LVINs (Figure 3D, F). For instance, each individual neuron in the lobula columnar LC15 subtype only connects to either or both PVLP.SCL.2 (PLP009 in hemibrain) and PVLP.SLP.13 (SLP306 in hemibrain), and each of these two LVINs primarily receive inputs from this cell type and not from other VPNs (Figure 3D, F). A similar situation exists in the case of MC62s: 97% of individual neurons of this type connect strongly to the LVIN

PLP251, and 7% also connect to either PLP231 or PLP120 (Figure 3D, F). In contrast to the LVINs downstream of LC15 that mostly receive input from LC15, the LVIN PLP251 also receives inputs from 19 other VPN types. In order to test for structure in these connectivity patterns in a more systematic way, we performed principal components analysis on the VPN-LVIN connectivity matrix (Figure 3E). We found that some principal components accounted for additional structure when compared to shuffled matrices preserving VPN connection probabilities and the number of inputs to each LVIN, demonstrating that these connections are inconsistent with a random model. The structured connectivity between VPNs and LVINs makes important predictions in terms of the degree of translational invariance that such a system might afford (see Discussion).

Receptive fields of neurons providing inputs to KCγ-d's

Some of the most distinctive features of visual neurons are the extent and location of their processes in the optic lobe neuropil they innervate. These are related to their receptive field size and position in the field of view of the animal. We used a newly developed 'eye-map', that allows the prediction of the receptive field of optic lobe neurons given the extent and location of their processes to extract receptive field size and position, to quantify these properties and relate them to their connectivity with KCγ-d's (Figure 4A)[50]. We first applied this methodology to direct and indirect VPNs from each neuropil to describe their individual receptive field properties and then extended our analysis to predict the visual receptive fields of individual KCγ-d's (Figure 4B, Figure 4 Supplement 1).

We found that for direct VPNs, especially in the case of medulla VPNs but also to a certain extent for aMe and lobula VPNs, the neurons that have the largest receptive fields are the ones that are the most strongly connected with KCγ-d's (Figure 4B, C, Figure 4 Supplement 1). This property holds to a lesser extent for indirect VPNs (Figure 4C, right). We next computed the location of the centroid of the receptive field of each VPN and plotted them on the eye map, as viewed by the left eye of the animal, weighted by the number of connections made by each VPN onto Kenyon cells (for direct VPNs) or by each VPN onto LVINs (for indirect VPNs) (Figure 4D, left; weight is indicated by size of the dot). We found that highly connected direct medulla VPNs preferentially represent the ventral part of the field of view of the fly, whereas highly connected direct lobula VPNs represent the dorsal part. Indirect lobula and medulla VPNs do not show this dorso-ventral distinction. Indirect aMe VPNs, however, preferentially represent the dorsal half of the field of view. We also noticed a slight rostral shift of lobula VPN centroids as compared to medulla VPNs, though this may reflect a technical limitation of the prediction tool. These properties are also apparent when overlaying the receptive fields of direct and indirect VPNs, separated between the three neuropils and weighted by the number of connections made by each VPN onto Kenyon cells or LVINs (shading) (Figure 4B).

Next we used these data to derive the putative receptive field of single KCγ-d's by linearly combining incident VPN and LVIN receptive fields and weighting by synaptic count. We show representative examples in Figure 4E. Overall, each KCγ-d samples most of the field of view of the animal and receives information from different parts of the visual field from different neuropils. The small size of the indirect VPN receptive fields is clearly apparent in some of these examples. The indirect receptive field composite images are combinations of LVIN receptive

fields. From this analysis we conclude that each KCγ-d receives non-stereotyped visual information, made up of combinations of VPNs, with direct VPNs encompassing larger parts of the field of view and indirect VPNs smaller parts of the field.

Individual KCγ-d's select inputs randomly from a precise set of visual neurons with heterogeneous weights

We next extended our analysis of the sets of inputs onto individual KCγ-d's to the whole population. We generated a matrix of connections onto each individual Kenyon cell in order to assess whether KCγ-d's receive labeled line, mixed, or randomized inputs (Figure 5A). Individual KCγ-d's received 1-7 visual inputs each, with a median of 3 (Figure 5B). Five identified KCγ-d's did not receive any inputs from VPNs or LVINs, and instead received input from olfactory PNs (Figure 5B). This median of 3 visual inputs per KCγ-d is slightly lower than the median 5-6 inputs received by olfactory Kenyon cells in general, and less than the 4-8 inputs that their closest developmental sisters, olfactory KCγ-main, receive in this brain[8,28,47]. We next analyzed the origin of inputs onto each cell (medulla, lobula, accessory medula or LVIN). Strikingly, all distributions of inputs were possible, from KCγ-d's receiving pure input from one neuropil to every mixture in between (Figure 5C).

Next, we asked whether specific inputs converged onto specific KCγ-d's by clustering KCγ-d's according to the inputs they received (Figure 5D, Figure 5 Supplement 1C). We did not see evidence of sorting or convergence in this data: KCγ-d's did not fall into obvious groups and knowing one input to a particular KCγ-d was not informative about other inputs. Hierarchical clustering performed on the matrix of connections onto KCγ-d's did not reveal any apparent structure, similar to the same procedure applied to KCγ-m's which receive distributed, combinatorial input from uniglomerular olfactory projection neurons (Figure 5 Supplement 1B-D). This contrasts with hierarchical clustering of inputs to individual olfactory projection neurons, which each receive convergent and deterministic input from dedicated olfactory sensory neurons in the antennal lobe (Figure 5 Supplement 1A).

A variety of methods have demonstrated the inputs to olfactory Kenyon cells in the adult are largely consistent with random sampling of locally available olfactory projection neuron boutons[7,28,51]. To further test for structure in the visual inputs to KCγ-d's, we examined the spectrum of the principal component eigenvalues of the Kenyon cell input covariance matrix, as has been done previously (Figure 5E-G)[7,13,28]. Comparing this spectrum to randomly shuffled controls provides a sensitive measure of whether particular patterns of input are overrepresented across the Kenyon cell population. We found no difference between the spectrum obtained from the EM reconstruction and shuffled spectra, consistent with random sampling of visual inputs. However, we find that the inputs to visual KCγ-d's are more skewed toward the top few input types than are olfactory inputs to Kenyon cells (Figure 5 Supplement 1E). To quantify this observation, we computed the predicted dimension of the visual input currents received by KCγ-d's, as quantified by the participation ratio[34,52], and compared it to that of the olfactory inputs to KCγ-m's. The participation ratio was lower in the case of visual connectivity compared to olfactory connectivity (visual: PR=9.1, olfactory: PR=15.4) despite the greater number of visual input channels, suggesting that visual inputs are dominated by a small number of input dimensions.

Nearly all uniglomerular olfactory projection neurons target the olfactory calyx with a probability of forming connections onto Kenyon cells that depends on glomerular and Kenyon cell types consistently across individuals within a species[7,8,30,31,53,54]. VPNs and LVINs are far more developmentally diverse than are olfactory projection neurons, and the neurons we identify projecting to the left vACA in FlyWire are only a tiny fraction of all VPNs (49 out of 3933 total left VPNs, ~1.2%). To ask if the same VPN and LVIN sets target the vACA between hemispheres, i.e. if this aspect of development is predictable, we generated a map of visual inputs to KCγ-d in the right hemisphere (Figure 6B). The top inputs to left and right hemispheres were the same, and neurons identified as KCγ-d inputs on only one hemisphere were of low rank in the hemisphere where they did connect (Figure 6A, B). Nevertheless, for 30/154 cell types that provided at least five synapses to the vACA in one hemisphere, we found that the paired cell type in the other hemisphere provided no calyx input even with the synapse threshold removed. These cells may be a source of inter-hemisphere or inter-individual variation in learnable visual signals.

To examine whether there is stereotypy in the specific combinations of these inputs that KCγ-d's in the left and right hemispheres sample, we asked whether there is an overrepresentation of left-right KCγ-d pairs that receive input from homologous visual inputs, as was previously done for olfactory inputs to larval KCγ-d's[13]. Of 147 KCγ-d cells in the left hemisphere, only 15 found a cell on the right hemisphere that received an identical set of visual inputs, no more than expected from shuffled connectivity matrices in which Kenyon cells in each hemisphere sample their inputs independently (Figure 6C). The principal component eigenvalues for the combined left-right input connectivity matrix also were not significantly different from those of shuffled models (Figure 6D).

Finally, to examine inter-individual variability, we repeated these analyses for homologous neurons identified in the hemibrain dataset. We used NBLAST[55] to query the morphology of each VPN and LVIN in our dataset against all neurons in the hemibrain volume (see Methods and results in Supplemental Table 3). Briefly, NBLAST is an algorithm that measures the similarity of two neuron structures, assigning them a similarity score between 0 and 1 (0=different neurons, 1=identical). We found confident matches in the hemibrain for 66% of VPN/LVINs in our dataset. These represent pairs of neurons with NBLAST scores greater than 0.5 (Figure 7A). We found that the number of synapses formed by VPNs and LVINs onto KCγ-d's are highly correlated across the two datasets (Figure 7B, C). As expected, principal components analysis found no evidence for stereotypy in these connections (Figure 7D). In conclusion, our analyses suggest that the connectivity between LVINs/VPNs and KCγ-d's is consistent with random sampling, but strongly biased toward specific input cell types which account for large proportions of visual information flow to these Kenyon cells.

Discussion

Striking heterogeneity in the visual inputs to the mushroom body

The insect mushroom body has long been studied for its role in chemosensory perception and associative odor learning, and as such the underlying circuits are well-described anatomically and functionally. Here we add to the rich knowledge of mushroom body olfactory coding by providing the first complete anatomic description of an

alternate sensory pathway to the adult mushroom bodies. Using the FlyWire electron microscopy reconstruction of the entire female adult fly brain, we have described all direct and indirect visual inputs (mono- and disynaptic connections) from the optic lobes to the ventral accessory calyx. By comparing the architectures of the olfactory and visual mushroom body circuits we highlight potential areas of functional similarity and difference.

Indeed, there are similarities between the olfactory and visual mushroom body circuits, including the distributed and random sampling of sensory inputs by Kenyon cells. Dissimilarities are most obvious at the level of cellular diversity and hint at possible functional differences in the way sensory modalities are used in the mushroom body during perception and learning. The olfactory projection neurons connected to the mushroom body receive inputs from the antennal lobe and are thus all positioned one synapse from the periphery. Olfactory projection neurons are born from dedicated stem cells and follow conserved tracts from the antennal lobe to the mushroom body calyx[56–59]. In contrast, the visual PNs that we have described here originate from multiple optic lobe neuropils. While the aMe12 neurons receive direct input from photoreceptors[16], medulla and lobula VPNs as well as LVINs are all at various depths of visual processing. Furthermore, single visual Kenyon cells can receive inputs from diverse mixtures of VPNs and LVINs; as a result, single visual Kenyon cells integrate visual information from various stages of visual processing. This anatomic arrangement differs from a model proposed in bees, that optic lobe sources would be sorted into different calyx regions[60].

VPNs make up a majority of the direct inputs to KCγ-d's; however, about a quarter of the synapses to KCγ-d's (and the majority of synapses to KCαβ-p's) are from LVINs that provide indirect visual input to the mushroom body. Many of the LVINs were first described by Li et al.[7], and here we identified the full repertoire of VPNs that are routed to the mushroom body via LVINs. LVINs integrate inputs from a large and diverse array of VPNs, especially when compared to VPNs that serve as direct inputs to Kenyon cells. For example, in the left hemisphere alone there are 49 VPNs that connect directly with KCγ-d's and 190 additional VPNs whose signals are routed to KCγ-d's via LVINs. Interestingly, 36/49 direct VPNs synapse with an LVIN, taking an indirect route to the mushroom body as well. The dual visual input from direct and indirect sources raises an interesting question about the functional role of each pathway type, and why most direct VPNs are also processed in parallel via the indirect pathway. Nevertheless, it is clear from an anatomic perspective that the LVINs are integrators of visual input, and in the future it will be interesting to further explore their functional role in visual processing.

What are Kenyon cells "seeing" and what are they using it for?

The similarity between the top VPN inputs to left and right hemispheres in the FlyWire dataset, as well as their similarity with VPNs in hemibrain, suggests that specific visual information is selected to be conveyed to the MB. Unfortunately, the great majority of the VPNs in question have not been studied, making it difficult to assign functions. Their anatomical characteristics however provide some indications as to stimulus preference. Many of the direct VPNs that we describe here sample broadly across the visual field, supporting the notion that this circuit is adapted for processing general features of a visual scene (e.g. luminance or color) rather than for encoding precise spatiotemporal relationships[61]. An interesting example is that of large-field aMe neurons, which make up 29.5% of VPN synapses onto KCγ-d's. While the role of aMe neurons has not been functionally determined, given

their position as inputs to circadian neurons it is likely that they could provide context to the mushroom body with information related to the time of day[62]. Despite the lack of overt spatial organization of the visual inputs in the mushroom body, there is precedent in other model systems for spatial encoding of stimuli in non-retinotopic circuits, which underscores the need for functional validation of these anatomic data[63]. Experiments aimed at probing stimulus selectivity of VPNs and Kenyon cells will be necessary to clarify the stimulus space to which the mushroom body is tuned.

In contrast, LVIN inputs to KCγ-d's process information from six kinds of lobular columnar (LC) neurons, amongst others. LCs are the main columnar output of the optic lobe, and are thought to each retinotopically encode different features of the visual scene[64–67]. For example, we have found that most members of the LC15 type, previously shown to respond specifically to long thin moving vertical bars[64,65], make connections with 1-2 LVINs. This suggests that a subset of KCγ-d's, receiving inputs from these particular LVINs, will respond to this particular stimulus, regardless of its location in the field of view of the animal. This convergent arrangement is ideal for providing translational invariance to stimuli in the mushroom body and therefore may contribute to visual learning about specific kinds of objects regardless of their spatial position.

KCγ-d's could be neural substrates for either pure visual learning and/or provide context for olfactory learning. There is substantial evidence for the latter. For instance, when a visual stimulus is paired with an odor, flies memorize these multisensory cues at higher rates compared to when the visual or olfactory stimuli are presented alone, a phenomenon that relies on KCγ-d activity[41,42]. This role in multisensory learning is further supported by anatomy. Indeed, in contrast to their separate inputs in the calyx, the axons of visual and olfactory Kenyon cells receive reinforcement from many common dopaminergic neurons (DANs) and synapse onto many common mushroom body output neurons (MBONs)[7,68]. Whereas most MBONs receive a large majority of olfactory inputs, reflecting the predominance of olfactory KCs, MBON19 and so-called "atypical" MBON27 and MBON33 receive a majority of their inputs from visual KCs, providing a potential substrate for a dedicated pathway for visual learning[7]. However, so far, a role for the mushroom body in pure visual learning in *Drosophila* is not clearly evident. In reinforcement paradigms where two color stimuli are presented and one is paired with either a reward or punishment, flies display a weak preference for either color in subsequent test trials[15,69]. However, it is not clear whether the colors tested activate separate populations of VPNs and consequently different subsets of visual KCs. Few visual stimuli have been tested in pure visual learning, and since our analysis shows that very specific visual neural types make their way to the mushroom body calyx, it is possible that extending the type of visual stimuli tested in associative learning paradigms will reveal significant mushroom body dependent visual learning.

Kenyon cells sample randomly from precisely allocated presynaptic inputs

The ~2000 Kenyon cells in the main olfactory calyx connect randomly to the ~50 types of olfactory projection neuron inputs[7,28,51]. The distributed nature of these connections expands the possible number of odors that can be encoded by the mushroom body[34]. As very different parameters compose a visual object vs. a smell (e.g. color, brightness, edges, line orientations, location, etc. versus molecular mixtures and concentrations), one may intuit

that the encoding of a visual percept in the mushroom body would inherently require a different circuit configuration. Instead, we find from examining the visual mushroom body connectivity in multiple hemispheres that, like olfactory Kenyon cells, visual Kenyon cells randomly sample from incoming VPNs and LVINs. This is predictive of a scenario in which the combinatorial coding of visual signals is used to generate visual percepts, yet if and how this type of coding scheme could generate coherent representations of visual objects is still unclear.

While the manner in which Kenyon cells connect to VPNs is random, the subset of VPNs included in this circuit seems relatively deterministic. In FlyWire, there are 7,851 total neurons annotated as VPNs. We find that just 469 of these 7,851 are direct or indirect visual inputs to KCγ-d's in left and right mushroom bodies. Among VPNs and LVINs connected directly to Kenyon cells, the top partners provide an outsized proportion of synaptic input, and the sharp differences in weights of these versus other inputs are consistent across hemispheres and brains. Much of this dominant input originates from accessory medulla neurons. The propensity for particular visual neurons to target the vACA, while others do not, suggests there are specific developmental instructions allowing these neurons to come into contact with KCγ-d's; once they do, the Kenyon cells sample randomly among them, seemingly agnostic to further features of LVIN or VPN identity. The adult KCγ-d set that we analyze here are the very same neurons that receive randomized olfactory input in the early larva, as these neurons prune their dendrites during metamorphosis before forming new, visual connections that will be used in the adult[13]. Though the random selection of inputs is a common feature of these cells across developmental time, their chosen partners switch from olfactory PNs for the larval circuit to this precise and diverse set of visual inputs for adulthood. What directs certain VPNs to synapse in the mushroom body and how Kenyon cells randomly select among these available partners will be interesting areas of future research.

Evolution of visual inputs to the mushroom body and visual learning

Across different insects, the size of the Kenyon cell repertoire and the balance of sensory modalities providing their input are highly divergent. In particular, species of *Hymenoptera*, *Lepidoptera*, and *Blattodea* have evolved ~100-fold expansions of the mushroom body, and these expansions are correlated with increased visual input and striking visual learning abilities[9]. The increase in visual Kenyon cell number and microglomerular structures in there species[9,70–72] correlate with with visual learning abilities that surpass what has been observed in flies: Many hymenopterans and lepidopterans use visual navigation to forage and particular species have also been shown to count, to recognize the faces of individual conspecifics, to be able to learn based on observation and inference, and to recognize visual cue configuration and abstraction[70,73–86]. However, the lack of genetic control in these species means a requirement for the mushroom body in visual learning has been addressed only rarely[15,44–46]. Therefore, the types of visual stimuli represented in the mushroom body, how visual percepts are encoded, and how these have been modified during evolution are unknown.

We show here that in flies, the mushroom body receives very specific channels of visual information: In the 80% of KCγ-d-inputs provided by VPNs, neurons representing full-field signals are prominent, while the 20% of inputs from LVINs include neurons representing small objects or specific kinds of motion. Among the insects with impressive visually-mediated behaviors there is a paucity of information about the exact neuron types and

connectivities that link the optic lobes to the mushroom bodies, though elaboration of visual Kenyon cell number in bees is proposed to occur together with re-routing of small-field visual signals to the mushroom body[87]. However, the overrepresentation of large-field inputs versus small-field inputs to the visual mushroom body that we observe in flies could be conserved across insects, and simply be mapped onto 500 times more visual Kenyon cells in Hymenopterans. In the future, comparative connectomic studies of insects with variation in visually mediated behaviors could begin to reveal how the evolution of circuits correlates with the emergence of sophisticated visual cognition.

Methods

Identification and characterization of direct visual inputs to visual Kenyon Cells in FlyWire

Data and accompanying annotations from the FlyWire v630 snapshot were used[8,47,48,88–91]. Our analyses used a ≥5 synapse threshold when determining a connection between neurons unless stated otherwise, in keeping consistent with connections indicated in Codex (https://codex.flywire.ai/). KCγ-d and KCαβ-p neurons were found in the FlyWire database by searching in Codex for "hemibrain_type = KCg-d" or "KCab-p." To identify the direct visual inputs to these neurons, we used the natverse R package (R version 4.3.1 (2023-06-16), RStudio Version 2023.06.1+524) and accompanying fafbseg library[92]. Using the function flywire_partner_summary2() and specifying version = "630" we queried all inputs to visual KCs in left and right hemispheres separately. We filtered the resulting inputs by neurons belonging to the "visual_projection" Super Class. Prior to filtering we noticed that not all the upstream neurons returned by flywire_partner_summary2() were given a Super Class designation; we therefore searched for these unclassified neurons individually in Codex to find their Super Class and included them in our dataset if they were annotated as visual projection neurons.

Neuropil origins of the visual projection neurons (VPNs) were largely determined based on noting the prefix of the neuron's cell name in Codex as well as visually inspecting where in the optic lobe most dendrites for a neuron were located. aME neurons were binned as such based on their given cell type classification in Codex.

Neurotransmitter (NT) identities were predicted by[90] and were found for each neuron through Codex. We report the predicted NT identity as was listed in Codex. Neurons predicted to be cholinergic generally had the highest confidence scores (>0.8).

Neuron names are generally reported as the Hemibrain Type when listed in Codex. When Hemibrain Type information was not available, we either reported the name as the Cell Type or the temporary name (e.g. SLP.208). A full list of neurons included in this study can be found in Supplementary Tables 1-3.

During its acquisition, the EM volume in FlyWire was flipped[47]. We present the left and right FlyWire hemispheres as their corrected versions as depicted in the Codex data explorer.

Identification of LVINs and indirect visual inputs to Kenyon Cells in FlyWire

Local Visual Interneurons (LVINs) were first described by Li et al., 2020[7]. They were defined as neurons that do not have processes in the optic lobes, receive input from VPNs, and synapse with Kenyon Cells. NBLAST[55] was initially used to map LVINs connected to KCγ-d's from the hemibrain to FlyWire. In FlyWire, all of these neurons belong to the "central" Super Class. We therefore searched for additional LVIN inputs to KCαβ-p's or KCγ-d's using the following filters: neurons belonging to the "central" Super Class (excluding Kenyon Cells, MBONs, DANs, APL, DPM, ALPNs), having ≥5 synapses with a single KCγ-d/αβ-p, and receiving input from visual projection neurons.

The indirect visual inputs to visual KCs were identified by querying the upstream inputs to each LVIN in Codex, filtered by "super_class = visual_projection." These cells were also filtered by having ≥5 synapses with a single LVIN unless stated otherwise.

When examining the resulting groups of indirect VPNs, we noticed that only a subset of some larger groups of neurons were synapsing with the LVINs. In the case of small-field Lobula Columnar neurons (LCs) which sample from discrete regions of visual space, this initially made it seem like an uneven and random assortment of visual space was being reported to the mushroom body. We checked if the ≥5 synapse threshold was masking the remaining inputs; we eliminated the synapse threshold by running flywire_partner_summary2(), querying inputs to KCγ-d without filtering by weight (i.e. synapses). This revealed the remaining neurons that make 4 or fewer synapses onto LVINs (Figure 3 Supplement 1).

Identification of putative KCγ-d synapse types

Olfactory projection neurons have axon collaterals that form synaptic bouton structures in the main mushroom body calyx. These boutons are enwrapped by the dendrites of Kenyon Cell claws. We examined the points of contact between VPN/LVIN axons and KCγ-d dendrites in the Codex 3D viewer and observed bouton-like terminals for both VPNs and LVINs that were enwrapped by KCγ-d dendrites. We designated these types of contacts as putative bouton-claw synapses. We also observed VPN/LVIN axons that were contacted along their length by a KCγ-d dendrite. We designated these as putative *en passant* synapses.

Morphological cell type clustering of neurons

All VPN and LVIN inputs on both hemispheres were taken into account during the clustering process. We used hierarchical clustering to group together neurons based on raw scores obtained from an all-by-all NBLAST run on all neuron skeletons. We then tuned clusters by eye by comparing morphologies and in some cases examining inputs, outputs, and hemilineages.

There are 6 neurons annotated as aMe26 in FlyWire (3 per hemisphere) but the neurons on left and right sides of the brain differ considerably in their morphology. Despite FlyWire calling these cells the same type, we chose to treat them as unique cell types based on our NBLAST clustering, and refer to these as aMe26_L and aMe26_R throughout the text and figures.

Comparing visual input organization to KCγ-d's between left and right hemispheres

Left-Right neuron morphology matches for direct VPNs and LVINs were identified in a stepwise manner. For some neurons in Codex, there is an assigned "mirror twin," or neuron that is the morphological match in the opposite hemisphere. Whenever this was the case, we chose this neuron to be the match. If there was no mirror twin listed for a neuron, we searched for all neurons that shared the same Hemibrain Type and assigned matching left-right pairs by eye. As a final step, if the neuron did not have a match through Codex we searched for a match among our list of neurons connected to KCγ-d's. For neurons where we could not easily query other cells of potentially similar morphology, we designated the match as "Unknown." For neurons that had a morphological match, we queried whether the match was also directly upstream of any KCγ-d's in the opposing hemisphere using a ≥5 synapse threshold. Upon doing so, we found that 45 neurons were unique to either the left or right mushroom body circuits. If we removed the synapse threshold, we were able to find the match for 15 of these 45 neurons in the opposing hemisphere. Following the process described above, we obtained 124 neurons with direct inputs to KCγ-d's across both hemispheres with putative matches in the opposite hemisphere. Since mirror twins were more ambiguous in the case of neurons within the same type class with very similar morphologies (e.g. aMe12), we condensed the matrix by cell type in some cases by averaging connectivity across direct VPNs and LVINs of the same morphological class.

To measure the extent of structure or randomness to the connectivity of direct VPNs and LVINs onto KCγ-d's between hemispheres, we first counted the pairs of KCγ-d's across hemispheres that received the same pattern of direct VPN and LVIN input (similar to analysis done in Eichler et al., 2017). Specifically, we counted how many KCγ-d's in the left hemisphere had an identical pattern of input to a KCγ-d in the right hemisphere; the total number of possible matches was 147, the number of KCγ-d's in the left hemisphere. Matches between hemispheres involving KCγ-d's receiving 0 inputs from our subsets of left-right matched VPNs and LVINs were not counted. We then compared the number of such matches we observed in the FlyWire dataset to the number of matches observed after shuffling both the left and right connectivity matrices while preserving VPN and LVIN connection probabilities and the number of inputs to each KCγ-d (1000 shuffled models were used; see Models of random connectivity).

We then used PCA to recover structure in direct VPN and LVIN connectivity to KCγ-d's after concatenating left and right connectivity matrices. We compared this structure to that obtained with random and stereotyped models of connectivity. For the random model, we shuffled connectivity across both hemispheres. In the stereotyped model, connectivity was shuffled in a randomly selected hemisphere and copied to the remaining hemisphere to generate identical but random connectivity in each hemisphere. In both models, shuffling was done preserving input connectivity distribution and the number of inputs sampled by each KCγ-d (see Models of random connectivity).

Estimating receptive fields of direct and indirect VPNs

Only visual projection neurons with optic lobe processes in the left hemisphere were considered for receptive field analyses. Columnar markers (759 in total) as identified in[50] were used. Since most medulla VPNs considered in this study arborize between layers M6 and M8, we used M5 column markers that were previously identified through the reconstruction of Mi1 processes in layer M5. Lobular column markers were obtained by extension of the medulla column map to the lobula from interpolating the positions of 63 reconstructed TmY5a neurons, as described in Zhao et al.[50]. Each columnar marker was mapped to an ommatidial viewing angle, directional vectors that were represented by points on a unit sphere (the "eyemap").

To estimate the receptive field of each VPN, we used morphological information available in the Flywire dataset to compute dendritic proximity to ommatidial columns within a specific distance threshold. We then computed the convex hull that encompassed this subset of ommatidial columns. A suitable threshold was set separately for lobular and medullar neurons by annotating receptive field edges by hand (visually selecting ommatidial columns) for a subset of ground truth neurons and choosing the threshold that maximized overlap between hand-drawn receptive fields and estimated receptive fields.

For all figures depicting receptive fields, a 2D Mollweide projection was used to portray the viewing directions of the ommatidial columns comprising the VPN's estimated receptive field. These viewing directions as well as midline and equatorial lines in visual space were determined in[50].

Matching neurons between FlyWire and Hemibrain volumes

To establish a mapping between FlyWire VPNs/LVINs and their counterparts in the hemibrain dataset, we used the fafbseg-py package (https://github.com/navis-org/fafbseg-py) to fetch and process FlyWire meshes for all neurons with cell bodies in the left hemisphere. We then used the transforms and brain templates available in navis-flybrains[92] to transform these FlyWire meshes to the hemibrain brain template (specifically the 'JRC2018F' template). As the FAFB brain was inverted during image acquisition, this transform aligned Flywire neurons from the left hemisphere with hemibrain neurons from the right hemisphere.

NBLAST[55] was used to query our subset of FlyWire neurons against all available neurons in the hemibrain dataset. The mean of the forward and reverse score was considered to obtain raw scores for each query-target pair. Each FlyWire neuron was paired with its highest scoring hemibrain match; in cases where two FlyWire neurons paired with the hemibrain neuron, the match with the stronger score was retained and the remaining neuron was paired with its next best NBLAST match. This process was repeated until a one-to-one mapping was obtained.

To probe if VPN/LVIN to KCγ-d connectivity was random between the two connectomes we used PCA to extract structure in an aggregated connectivity matrix containing direct VPN/LVIN to KCγ-d connectivity from one hemisphere of FlyWire and one hemisphere of hemibrain. Using a similar approach to the analysis comparing left and right hemisphere connectivity (see Comparing visual input organization to KCγ-d's between left and right hemispheres), we compared the observed structure with a random model shuffling connectivity across both

connectomes. In the stereotyped model, connectivity was shuffled in one of the connectomes and copied to the remaining hemisphere to generate identical but random connectivity in each hemisphere.

Random models of VPN/LVIN-KC connectivity

To determine if there was any structure in connectivity that wasn't accounted for by the non-uniform distribution of input connection probabilities or the non-uniform number of inputs to each output neuron, we used a shuffle procedure where the connection probabilities of inputs and the number of inputs to each postsynaptic output were fixed. PCA was used to extract correlations in connectivity matrices such as VPN connectivity to LVINs or direct VPN/LVIN connectivity to KCγ-d's. The fractions of variance explained by the top components were compared with those obtained with a set of randomly generated connectivity matrices using this shuffle procedure[28]. For each figure exploring the extent of random connectivity in this study, data was compared to 1,000 random shuffles.

Clustering KCγ-d's using connectivity

Spectral clustering was applied to binarized direct VPN and LVIN to KCγ-d connectivity in an attempt to group KCγ-d's into clusters. The optimal number of clusters (4 clusters) was selected by computing the silhouette score as a measure of clustering accuracy over a range of cluster numbers and selecting the number of clusters with the best score.

Data visualization

Images of neuron and brain anatomy were generated through Codex using the 3D viewer. The CNS brain mesh used throughout the figures are from the codex layer "brain_mesh_v3." The brain mesh and the accompanying neuropils highlighted in Figure 2 were generated by Schlegel et al., 2023 based on FlyWire synapse data[47,89].

Heatmaps in Figure 5 Supplement 1 were made using the fafbseg R package from natverse [92] (R version 4.3.1 (2023-06-16), RStudio Version 2023.06.1+524). Adjacency matrices were first generated for groups of input and output neurons using the flywire_adjacency_matrix() function. The resulting connectivity matrix was then binarized so that every neuron-neuron contact with ≥5 synapses was set to 1 and any contact of 0-4 synapses was set to 0. The binarized matrix was plotted using the standard R heatmap() function, which also hierarchically clustered the rows and columns based on the similarity of their synaptic partners. As inputs we used neuroglancer scenes from the production dataset (ngl.flywire.ai) depicting olfactory receptor neurons with input to the left antennal lobe; uniglomerular PNs that receive input in the left antennal lobe; KCγ-m's in the left hemisphere; LVINs and VPNs that provide direct input to the left hemisphere KCγ-d's; and KCγ-d's in the left hemisphere.

Remaining plots were made using a combination of Google Sheets and standard Python plotting packages (Matplotlib, Seaborn).

Acknowledgements

We thank the Princeton FlyWire team and members of the Murthy and Seung labs, as well as members of the Allen Institute for Brain Science, for development and maintenance of FlyWire (supported by BRAIN Initiative grants MH117815 and NS126935 to Murthy and Seung). We also acknowledge members of the Princeton FlyWire team and the FlyWire consortium for neuron proofreading and annotation. Natverse R and Python packages [92] were relied on for querying connectivity and generating data visualizations. Development of the natverse including the fafbseg package was supported by the NIH BRAIN Initiative (grant 1RF1MH120679-01), NSF/MRC Neuronex2 (NSF 2014862/MC_EX_MR/T046279/1) and core funding from the Medical Research Council (MC_U105188491). We thank Alvaro Sanz-Diez for help with validation of the neural type clustering. Funding was provided by NIDCD R01DC018032, the Pew Charitable Trusts, the McKnight Endowment Fund, the Rita Allen Foundation, and the University of Michigan to E.J.C.; Hearing, Balance, and Chemical Senses Training Program (T32-DC000011) and HHMI Hanna Gray Fellowship to E.L.H.; DOE CSGF (DESC0022158) and the Gastby Charitable Foundation to I.G.; BRAIN R34NS128874, NIH R01EY029311, the Mathers Foundation, the Pew Charitable Trusts, the McKnight Endowment Fund, the Grossman Charitable Trust and the Kavli Foundation to R.B. ; A.L.-K. was supported by the Burroughs Wellcome Foundation, the Gatsby Charitable Foundation, the McKnight Endowment Fund, and NIH award R01EB029858.

Supplementary Information

Supplementary Table 1. KCγ-d Visual Inputs.

A list of all FlyWire visual projection neurons (VPNs) and local visual interneurons (LVINs) with direct or indirect input to KCγ-d neurons (≥5 synapse threshold). FlyWire neuron IDs are given for each neuron from the version 630 snapshot of the data, and when applicable, the updated version of the ID as of October 5, 2023. When able, we supply the ID of the neuron match in the opposing hemisphere (i.e. Mirror Twin). NBLAST cluster IDs for all direct inputs as well as left hemisphere indirect inputs are given.

Supplementary Table 2. KCαβ-p Visual Inputs.

A list of all FlyWire visual projection neurons (VPNs) and local visual interneurons (LVINs) with direct input to KCαβ-p neurons (≥5 synapse threshold). FlyWire neuron IDs are given for each neuron from the version 630 snapshot of the data, and when applicable, the updated version of the ID as of October 5, 2023. We identify the cells that are also inputs to KCγ-d.

Supplementary Table 3. Hemibrain-FlyWire Matches.

A list of all FlyWire visual projection neurons (VPNs) and local visual interneurons (LVINs) with direct or indirect input to KCγ-d neurons (≥5 synapse threshold) along with their putative matches in the Hemibrain dataset obtained by computing NBLAST scores. Raw NBLAST scores are reported. The total number of direct

synapses each neuron makes onto the KCγ-d population in both the FlyWire and Hemibrain datasets as well as the Hemibrain Types are included. FlyWire neuron IDs for each neuron are from the version 630 snapshot.

References

1. Aso, Y. *et al.* Mushroom body output neurons encode valence and guide memory-based action selection in Drosophila. *eLife* **3**, e04580 (2014).
2. Aso, Y. & Rubin, G. M. Dopaminergic neurons write and update memories with cell-type-specific rules. *eLife* **5**, e16135 (2016).
3. Cohn, R., Morantte, I. & Ruta, V. Coordinated and Compartmentalized Neuromodulation Shapes Sensory Processing in Drosophila. *Cell* **163**, 1742–1755 (2015).
4. Hige, T., Aso, Y., Modi, M. N., Rubin, G. M. & Turner, G. C. Heterosynaptic Plasticity Underlies Aversive Olfactory Learning in Drosophila. *Neuron* **88**, 985–998 (2015).
5. Owald, D. *et al.* Activity of defined mushroom body output neurons underlies learned olfactory behavior in Drosophila. *Neuron* **86**, 417–427 (2015).
6. Perisse, E. *et al.* Aversive Learning and Appetitive Motivation Toggle Feed-Forward Inhibition in the Drosophila Mushroom Body. *Neuron* **90**, 1086–1099 (2016).
7. Li, F. *et al.* The connectome of the adult Drosophila mushroom body provides insights into function. *eLife* **9**, e62576 (2020).
8. Zheng, Z. *et al.* A Complete Electron Microscopy Volume of the Brain of Adult Drosophila melanogaster. *Cell* **174**, 730-743.e22 (2018).
9. Farris, S. M. Evolution of brain elaboration. *Philos Trans R Soc Lond B Biol Sci* **370**, 20150054 (2015).
10. Aso, Y. *et al.* The mushroom body of adult Drosophila characterized by GAL4 drivers. *Journal of Neurogenetics* **23**, 156–172 (2009).
11. Puñal, V. M., Ahmed, M., Thornton-Kolbe, E. M. & Clowney, E. J. Untangling the wires: development of sparse, distributed connectivity in the mushroom body calyx. *Cell Tissue Res* **383**, 91–112 (2021).
12. Technau, G. & Heisenberg, M. Neural reorganization during metamorphosis of the corpora pedunculata in Drosophila melanogaster. *Nature* **295**, 405–407 (1982).
13. Eichler, K. *et al.* The complete connectome of a learning and memory centre in an insect brain. *Nature* **548**, 175–182 (2017).
14. Pauls, D., Selcho, M., Gendre, N., Stocker, R. F. & Thum, A. S. Drosophila larvae establish appetitive olfactory memories via mushroom body neurons of embryonic origin. *J. Neurosci.* **30**, 10655–10666 (2010).
15. Vogt, K. *et al.* Direct neural pathways convey distinct visual information to drosophila mushroom bodies. *eLife* **5**, 1–13 (2016).
16. Kind, E. *et al.* Synaptic targets of photoreceptors specialized to detect color and skylight polarization in Drosophila. *Elife* **10**, e71858 (2021).
17. Li, J., Mahoney, B. D., Jacob, M. S. & Caron, S. J. C. Visual Input into the Drosophila melanogaster

Mushroom Body. *Cell reports* **32**, 108138–108138 (2020).

18. Tanaka, N. K., Tanimoto, H. & Ito, K. Neuronal assemblies of the Drosophila mushroom body. *The Journal of comparative neurology* **508**, 711–55 (2008).
19. Hofbauer, A. & Buchner, E. Does Drosophila have seven eyes? *Naturwissenschaften* **76**, 335–336 (1989).
20. Damulewicz, M. & Pyza, E. The Clock Input to the First Optic Neuropil of Drosophila melanogaster Expressing Neuronal Circadian Plasticity. *PLOS ONE* **6**, e21258 (2011).
21. Helfrich-Förster, C. *et al.* Development and morphology of the clock-gene-expressing lateral neurons of Drosophila melanogaster. *Journal of Comparative Neurology* **500**, 47–70 (2007).
22. Schlichting, M. *et al.* Light-Mediated Circuit Switching in the Drosophila Neuronal Clock Network. *Current Biology* **29**, 3266-3276.e3 (2019).
23. Veleri, S., Rieger, D., Helfrich-Förster, C. & Stanewsky, R. Hofbauer-Buchner eyelet affects circadian photosensitivity and coordinates TIM and PER expression in Drosophila clock neurons. *J Biol Rhythms* **22**, 29–42 (2007).
24. Helfrich-förster, C., Stengl, M. & Homberg, U. Organization of the Circadian System in Insects. *Chronobiology International* **15**, 567–594 (1998).
25. Scheffer, L. K. *et al.* A connectome and analysis of the adult Drosophila central brain. *eLife* **9**, e57443 (2020).
26. Bates, A. S. *et al.* Complete Connectomic Reconstruction of Olfactory Projection Neurons in the Fly Brain. *Current Biology* **30**, 3183-3199.e6 (2020).
27. Butcher, N. J., Friedrich, A. B., Lu, Z., Tanimoto, H. & Meinertzhagen, I. A. Different classes of input and output neurons reveal new features in microglomeruli of the adult Drosophila mushroom body calyx. *J Comp Neurol* **520**, 2185–2201 (2012).
28. Caron, S. J. C., Ruta, V., Abbott, L. F. & Axel, R. Random convergence of olfactory inputs in the Drosophila mushroom body. *Nature* **497**, 113–117 (2013).
29. Leiss, F., Groh, C., Butcher, N. J., Meinertzhagen, I. A. & Tavosanis, G. Synaptic organization in the adult Drosophila mushroom body calyx. *The Journal of comparative neurology* **517**, 808–24 (2009).
30. Marin, E. C., Jefferis, G. S. X. E., Komiyama, T., Zhu, H. & Luo, L. Representation of the glomerular olfactory map in the Drosophila brain. *Cell* **109**, 243–255 (2002).
31. Wong, A. M., Wang, J. W. & Axel, R. Spatial representation of the glomerular map in the Drosophila protocerebrum. *Cell* **109**, 229–241 (2002).
32. Ahmed, M. *et al.* Input density tunes Kenyon cell sensory responses in the Drosophila mushroom body. *Curr Biol* **33**, 2742-2760.e12 (2023).
33. Gruntman, E. & Turner, G. C. Integration of the olfactory code across dendritic claws of single mushroom body neurons. *Nature neuroscience* **16**, 1821–9 (2013).
34. Litwin-Kumar, A., Harris, K. D., Axel, R., Sompolinsky, H. & Abbott, L. F. Optimal Degrees of Synaptic Connectivity. *Neuron* **93**, 1153-1164.e7 (2017).
35. Vogt, K., Yarali, A. & Tanimoto, H. Reversing Stimulus Timing in Visual Conditioning Leads to Memories with Opposite Valence in Drosophila. *PLoS One* **10**, e0139797 (2015).
36. Vogt, K. *et al.* Shared mushroom body circuits underlie visual and olfactory memories in Drosophila. *Elife*

3, e02395 (2014).

37. Liu, L., Wolf, R., Ernst, R. & Heisenberg, M. Context generalization in Drosophila visual learning requires the mushroom bodies. *Nature* **400**, 753–756 (1999).
38. Ofstad, T. A., Zuker, C. S. & Reiser, M. B. Visual place learning in Drosophila melanogaster. *Nature* **474**, 204–207 (2011).
39. Liu, G. *et al.* Distinct memory traces for two visual features in the Drosophila brain. *Nature* **439**, 551–556 (2006).
40. Wang, Z. *et al.* Visual pattern memory requires foraging function in the central complex of Drosophila. *Learn Mem* **15**, 133–142 (2008).
41. Guo, J. & Guo, A. Crossmodal interactions between olfactory and visual learning in Drosophila. *Science* **309**, 307–310 (2005).
42. Okray, Z. *et al.* Multisensory learning binds neurons into a cross-modal memory engram. *Nature* **617**, 777–784 (2023).
43. Zhang, X., Ren, Q. & Guo, A. Parallel pathways for cross-modal memory retrieval in Drosophila. *J Neurosci* **33**, 8784–8793 (2013).
44. Buehlmann, C. *et al.* Mushroom Bodies Are Required for Learned Visual Navigation, but Not for Innate Visual Behavior, in Ants. *Current Biology* **30**, 3438-3443.e2 (2020).
45. Mizunami, M., Weibrecht, J. M. & Strausfeld, N. J. Mushroom bodies of the cockroach: their participation in place memory. *J Comp Neurol* **402**, 520–537 (1998).
46. Plath, J. A. *et al.* Different Roles for Honey Bee Mushroom Bodies and Central Complex in Visual Learning of Colored Lights in an Aversive Conditioning Assay. *Frontiers in Behavioral Neuroscience* **11**, (2017).
47. Schlegel, P. *et al.* Whole-brain annotation and multi-connectome cell typing quantifies circuit stereotypy in Drosophila. *bioRxiv* 2023.06.27.546055 (2023) doi:10.1101/2023.06.27.546055.
48. Dorkenwald *et al.* Neuronal wiring diagram of an adult brain. *bioRxiv* 2023.06.27.546656 (2023) doi:10.1101/2023.06.27.546656.
49. Jefferis, G. S. X. E. *et al.* Comprehensive maps of Drosophila higher olfactory centers: spatially segregated fruit and pheromone representation. *Cell* **128**, 1187–1203 (2007).
50. Zhao *et al.* Eye structure shapes neuron function in Drosophila motion vision. *bioRxiv* 2022.12.14.520178 (2022) doi:10.1101/2022.12.14.520178.
51. Murthy, M., Fiete, I. & Laurent, G. Testing Odor Response Stereotypy in the Drosophila Mushroom Body. *Neuron* **59**, 1009–1023 (2008).
52. Peiran Gao *et al.* A theory of multineuronal dimensionality, dynamics and measurement. *bioRxiv* 214262 (2017) doi:10.1101/214262.
53. Ellis, K. E. *et al.* Evolution of connectivity architecture in the Drosophila mushroom body. *bioRxiv* 2023.02.10.528036 (2023) doi:10.1101/2023.02.10.528036.
54. Tanaka, N. K., Awasaki, T., Shimada, T. & Ito, K. Integration of Chemosensory Pathways in the Drosophila Second-Order Olfactory Centers. *Current Biology* **14**, 449–457 (2004).
55. Costa, M., Manton, J. D., Ostrovsky, A. D., Prohaska, S. & Jefferis, G. S. X. E. NBLAST: Rapid, Sensitive

Comparison of Neuronal Structure and Construction of Neuron Family Databases. *Neuron* **91**, 293–311 (2016).

56. Galizia, C. G. & Rössler, W. Parallel Olfactory Systems in Insects: Anatomy and Function. *Annual Review of Entomology* **55**, 399–420 (2010).
57. Ito, K. *et al.* The organization of extrinsic neurons and their implications in the functional roles of the mushroom bodies in Drosophila melanogaster meigen. *Learning and Memory* **5**, 52–77 (1998).
58. Stocker, R. F., Heimbeck, G., Gendre, N. & de Belle, J. S. Neuroblast ablation in Drosophila P[GAL4] lines reveals origins of olfactory interneurons. *Journal of neurobiology* **32**, 443–56 (1997).
59. Stocker, R. F., Lienhard, M. C., Borst, A. & Fischbach, K. F. Neuronal architecture of the antennal lobe in Drosophila melanogaster. *Cell and Tissue Research* **262**, 9–34 (1990).
60. Ehmer, B. & Gronenberg, W. Segregation of visual input to the mushroom bodies in the honeybee (Apis mellifera). *Journal of Comparative Neurology* **451**, 362–373 (2002).
61. Currier, T. A., Pang, M. M. & Clandinin, T. R. Visual processing in the fly, from photoreceptors to behavior. *Genetics* **224**, iyad064 (2023).
62. Nils Reinhard *et al.* Synaptic and peptidergic connectomes of the Drosophila circadian clock. *bioRxiv* 2023.09.11.557222 (2023) doi:10.1101/2023.09.11.557222.
63. Fournier, J., Müller, C. M., Schneider, I. & Laurent, G. Spatial Information in a Non-retinotopic Visual Cortex. *Neuron* **97**, 164-180.e7 (2018).
64. Klapoetke, N. C. *et al.* A functionally ordered visual feature map in the Drosophila brain. *Neuron* **110**, 1700-1711.e6 (2022).
65. Städele, C., Keleş, M. F., Mongeau, J.-M. & Frye, M. A. Non-canonical Receptive Field Properties and Neuromodulation of Feature-Detecting Neurons in Flies. *Curr Biol* **30**, 2508-2519.e6 (2020).
66. Turner, M. H., Krieger, A., Pang, M. M. & Clandinin, T. R. Visual and motor signatures of locomotion dynamically shape a population code for feature detection in Drosophila. *eLife* **11**, e82587 (2022).
67. Wu, M. *et al.* Visual projection neurons in the Drosophila lobula link feature detection to distinct behavioral programs. *eLife* **5**, e21022 (2016).
68. Aso, Y. *et al.* The neuronal architecture of the mushroom body provides a logic for associative learning. *Elife* **3**, e04577 (2014).
69. Schnaitmann, C., Vogt, K., Triphan, T. & Tanimoto, H. Appetitive and aversive visual learning in freely moving Drosophila. *Frontiers in Behavioral Neuroscience* **4**, (2010).
70. Couto, A. *et al.* Rapid expansion and visual specialisation of learning and memory centres in the brains of Heliconiini butterflies. *Nat Commun* **14**, 4024 (2023).
71. Groh, C. & Rössler, W. Comparison of microglomerular structures in the mushroom body calyx of neopteran insects. *Arthropod Struct Dev* **40**, 358–367 (2011).
72. Li, L. *et al.* A possible structural correlate of learning performance on a colour discrimination task in the brain of the bumblebee. *Proceedings of the Royal Society B: Biological Sciences* **284**, 20171323 (2017).
73. Alem, S. *et al.* Associative Mechanisms Allow for Social Learning and Cultural Transmission of String Pulling in an Insect. *PLOS Biology* **14**, e1002564 (2016).
74. Becker, L. Untersuchungen über das Heimfindevermögen der Bienen. *Zeitschrift für vergleichende*

Physiologie **41**, 1–25 (1958).

75. Bridges, A. D. *et al.* Bumblebees acquire alternative puzzle-box solutions via social learning. *PLOS Biology* **21**, e3002019 (2023).
76. Dacke, M. & Srinivasan, M. V. Evidence for counting in insects. *Anim Cogn* **11**, 683–689 (2008).
77. Degen, J. *et al.* Honeybees Learn Landscape Features during Exploratory Orientation Flights. *Current Biology* **26**, 2800–2804 (2016).
78. Giurfa, M., Zhang, S., Jenett, A., Menzel, R. & Srinivasan, M. V. The concepts of 'sameness' and 'difference' in an insect. *Nature* **410**, 930–933 (2001).
79. Graham, P. & Philippides, A. Vision for navigation: What can we learn from ants? *Arthropod Struct Dev* **46**, 718–722 (2017).
80. Gross, H. J. *et al.* Number-Based Visual Generalisation in the Honeybee. *PLoS One* **4**, e4263 (2009).
81. Sheehan, M. J. & Tibbetts, E. A. Specialized Face Learning Is Associated with Individual Recognition in Paper Wasps. *Science* **334**, 1272–1275 (2011).
82. Tibbetts, E. A., Wong, E. & Bonello, S. Wasps Use Social Eavesdropping to Learn about Individual Rivals. *Current Biology* **30**, 3007-3010.e2 (2020).
83. Wehner, R., Cheng, K. & Cruse, H. Visual navigation strategies in insects: lessons from desert ants. in *The New visual neurosciences* (eds. Werner, J. S. & Chalupa, L. M.) 1153–1163 (The MIT Press, 2014).
84. Weise, C., Ortiz, C. C. & Tibbetts, E. A. Paper wasps form abstract concept of 'same and different'. *Proceedings of the Royal Society B: Biological Sciences* **289**, 20221156 (2022).
85. Worden, B. D. & Papaj, D. R. Flower choice copying in bumblebees. *Biology Letters* **1**, 504–507 (2005).
86. Zeil, J. Visual homing: an insect perspective. *Current Opinion in Neurobiology* **22**, 285–293 (2012).
87. Paulk, A. C. & Gronenberg, W. Higher order visual input to the mushroom bodies in the bee, Bombus impatiens. *Arthropod Struct Dev* **37**, 443–458 (2008).
88. Buhmann, J. *et al.* Automatic detection of synaptic partners in a whole-brain Drosophila electron microscopy data set. *Nat Methods* **18**, 771–774 (2021).
89. Dorkenwald, S. *et al.* FlyWire: online community for whole-brain connectomics. *Nat Methods* **19**, 119–128 (2022).
90. Eckstein *et al.* Neurotransmitter Classification from Electron Microscopy Images at Synaptic Sites in Drosophila Melanogaster. *bioRxiv* 2020.06.12.148775 (2023) doi:10.1101/2020.06.12.148775.
91. Heinrich, L., Funke, J., Pape, C., Nunez-Iglesias, J. & Saalfeld, S. Synaptic Cleft Segmentation in Non-isotropic Volume Electron Microscopy of the Complete Drosophila Brain. in *Medical Image Computing and Computer Assisted Intervention – MICCAI 2018* (eds. Frangi, A. F., Schnabel, J. A., Davatzikos, C., Alberola-López, C. & Fichtinger, G.) 317–325 (Springer International Publishing, 2018). doi:10.1007/978-3-030-00934-2_36.
92. Bates *et al.* The natverse, a versatile toolbox for combining and analysing neuroanatomical data. *eLife* **9**, e53350 (2020).

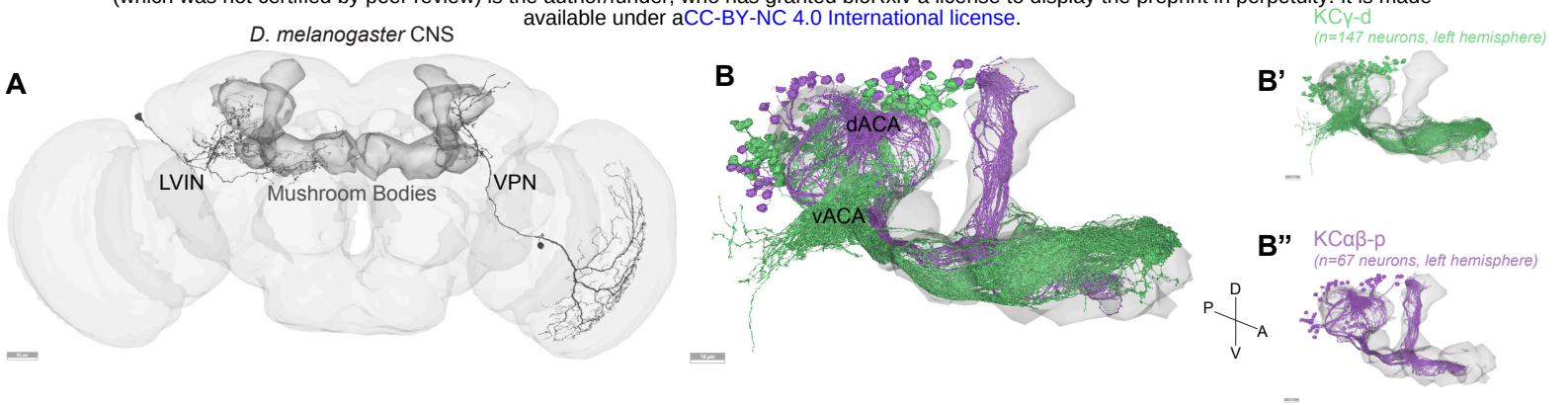

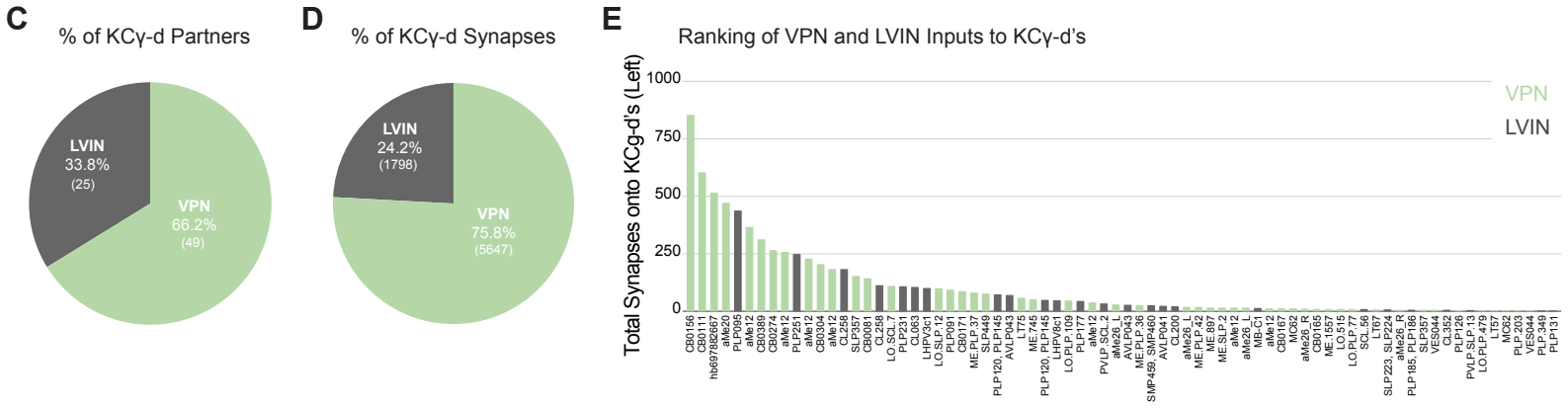

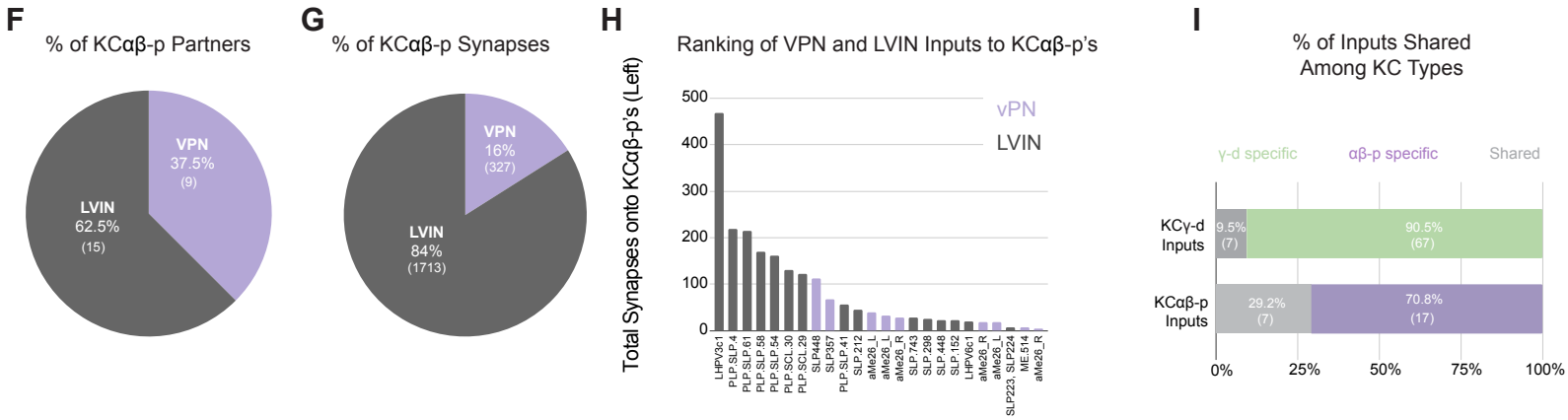

Figure 1. Direct visual inputs are highly represented in the ventral accessory calyx.

A. Schematic of the *D. melanogaster* CNS with the mushroom bodies highlighted in dark gray. Representative examples of an LVIN (PLP095) and VPN (CB0156). Anterior view. Scale bar, 30µm.

B. Mushroom body volume with visual Kenyon cell subtypes overlaid. dACA, dorsal accessory calyx, vACA, ventral accessory calyx. (B') KCγ-d, green receives input in the vACA. (B") KCαβ-p, purple, receives input in the dACA. Scale bar, 15µm.

C. Proportion of KCγ-d visual inputs that are either VPNs (green) or LVINs (gray).

D. Proportion of visual synapses onto KCγ-d that are either from VPNs or LVINs.

E. Ranking all VPN and LVIN inputs to KCγ-d by their total synaptic contribution to KCγ-d's.

F. Proportion of KCαβ-p visual inputs that are either VPNs (purple) or LVINs (gray).

G. Proportion of visual synapses onto KCαβ-p that are either from VPNs or LVINs.

H. Ranking all VPN and LVIN inputs to KCαβ-p by their total synaptic contribution to KCαβ-p's.

I. Proportion of direct visual inputs and LVINs that are either specific to or shared among KCγ-d and KCαβ-p.

All data in panels B-I examine connectivity in the left hemisphere, using a ≥5 synapse threshold.

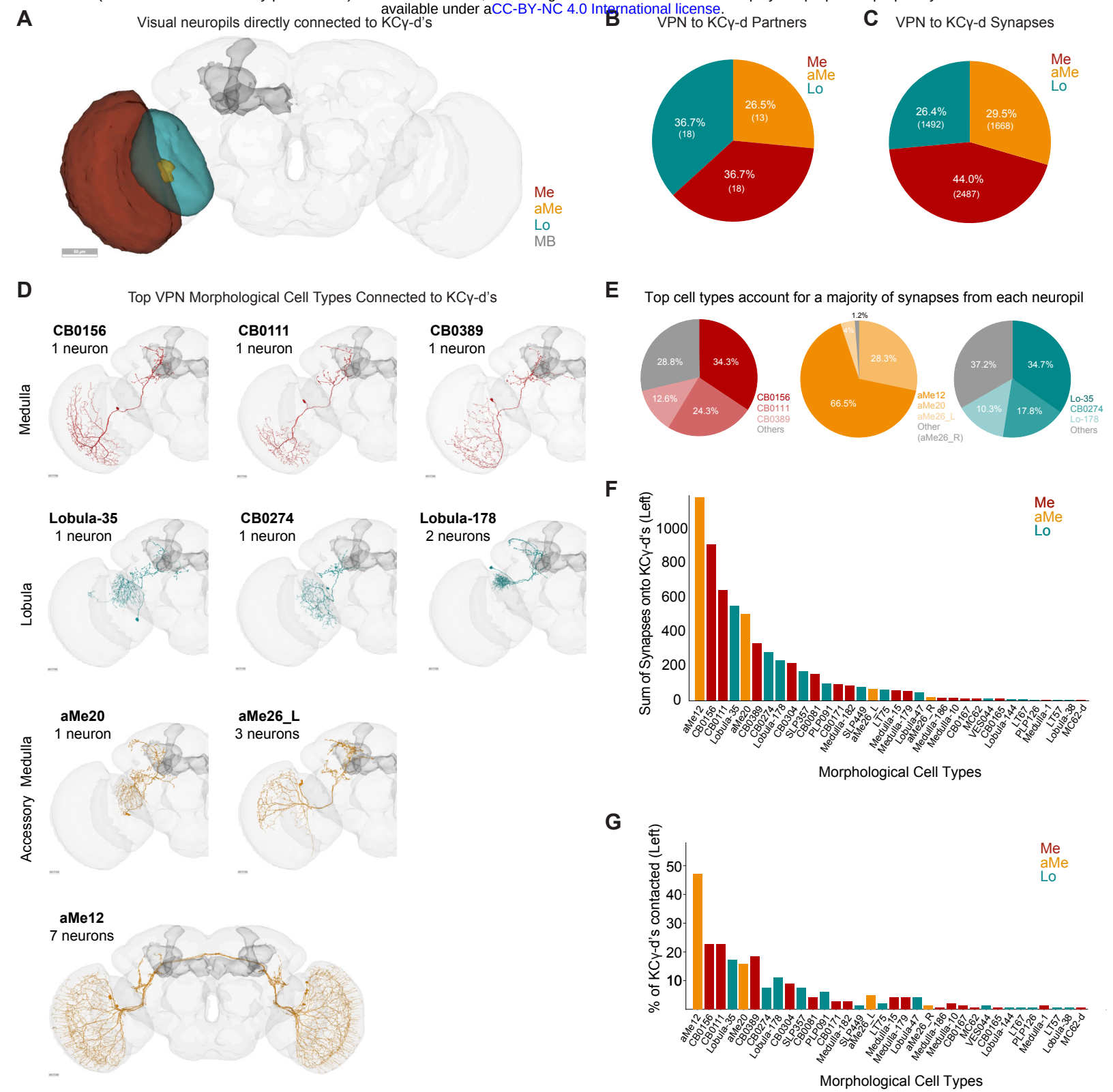

Figure 2. Direct visual inputs to KCγ-d neurons come from diverse optic lobe neuropils.

A. Schematic of optic lobe neuropils and mushroom body in the left hemisphere. The same neuropils are present in the right hemisphere but are not highlighted here. Me, Medulla; aMe, Accessory Medulla; Lo, Lobula; MB, Mushroom Body. Scale bar, 50μm.

B. Proportion of KCγ-d VPN partners that originate from one of the 3 optic lobe neuropils in (A).

C. Proportion of VPN synapses onto KCγ-d by optic lobe neuropil origin.

D. Morphologies of the top three VPN classes from each neuropil that provide the most synaptic input to KCγ-d's. Scale bars, 20μm.

E. Proportion of synapses from each neuropil that come from the top 3 morphological types in (D).

F. Ranking of morphological VPN classes by total synaptic contribution to KCγ-d's.

G. Percentage of KCγ-d's contacted by each morphological VPN class (out of 147 KCγ-d's in the left hemisphere). VPN classes are ordered on the x-axis as in (F) to show that classes making larger numbers of synapses also contact larger percentages of KCγ-d partners.

Data in this figure examine connectivity in the left hemisphere, using a ≥5 synapse threshold.

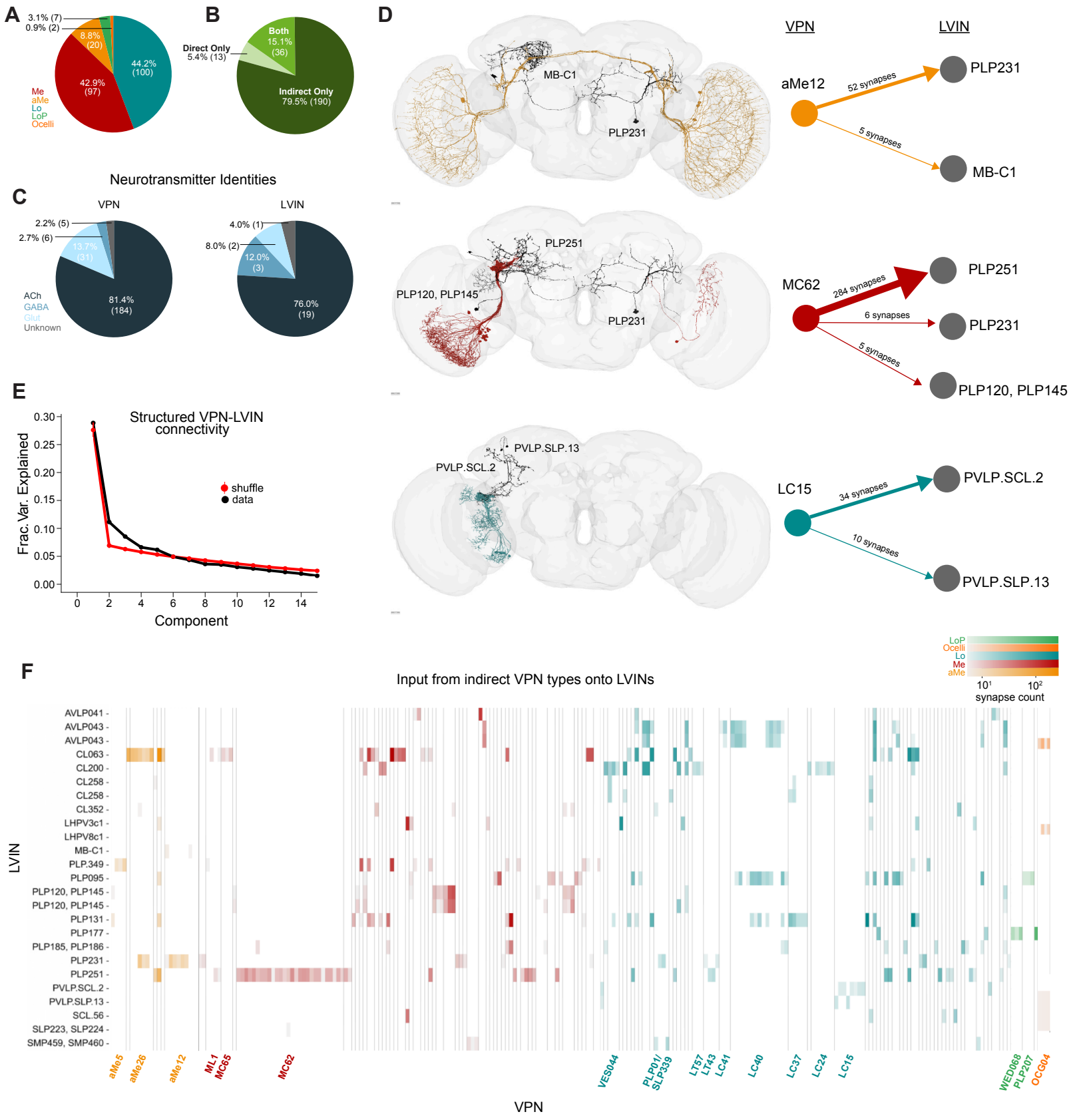

Figure 3. LVINs relay structured visual inputs to KCγ-d.

A. Proportion of indirect VPNs that originate from a given neuropil origin. Me, Medulla; aMe, Accessory Medulla; Lo, Lobula; LoP, Lobula Plate.

B. Proportion of VPNs in our dataset that provide only direct, only indirect (via LVINs), or both direct and indirect input to KCγ-d's.

C. Predicted neurotransmitter identities (Eckstein, Bates, et al., 2023) for indirect VPNs (left) and LVINs (right). ACh, acetylcholine; Glut, glutamate.

D. Examples of indirect VPNs that demonstrate a bias for certain LVINs. aMe12s (top) mostly target the LVIN PLP231, with one aMe12 targeting MB-C1. Most MC62s (middle) converge onto the LVIN PLP251. One MC62 from the right hemisphere contacts PLP231 which in turn synapses onto KCγ-d in the left hemisphere. LC15s synapse onto PVLP.SCL.2 and PVLP.SLP.13. Scale bars 15μm.

E. Principal components analysis of indirect VPN to LVIN connectivity. Red circles and bars represent mean and 95% confidence intervals for the variance explained by the principal components of shuffled connectivity matrices where VPN connection probabilities and number of inputs to each LVIN are preserved. Top PC components account for more structure than shuffled matrices.

F. Connectivity matrix examining inputs from indirect VPNs onto LVINs. VPNs are organized by input neuropil and morphological type and LVINs are organized by morphological type. Indirect VPN classes that correspond to previously named morphological types and contain three or more neurons are labeled. Individual LVINs and LVIN classes receive structured inputs from specific VPN classes.

Data in this figure examine connectivity in the left hemisphere, using a ≥5 synapse threshold.

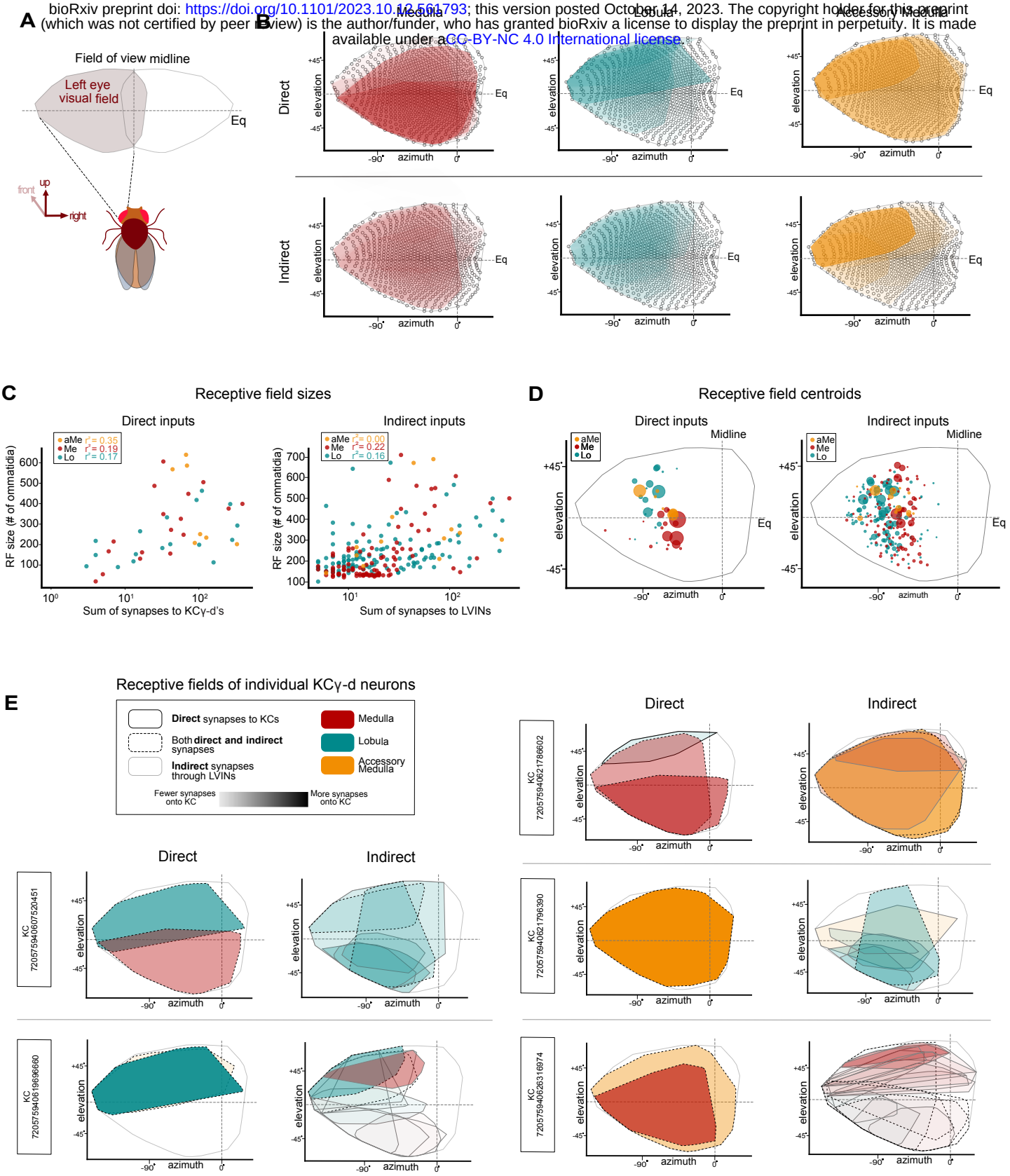

Figure 4. Receptive fields of direct and indirect VPNs.

A. Schematic illustrating the region of visual space sampled by ommatidia in the left eye. The region above the equator (elevation > 0°) and below the equator (elevation < 0°) represent the dorsal and ventral half of the visual field respectively.

B. Right top, for each input neuropil, estimated receptive fields (Mollweide projections of ommatidial viewing angles) of each direct VPN input are overlaid. Shading of each individual receptive field indicates the proportion of synaptic input onto the KCγ-d population. Right bottom, estimated receptive fields of each indirect VPN input are overlaid for each input neuropil. Shading of each individual receptive field indicates the proportion of synaptic input onto the KCγ-d population, obtained by multiplying VPN-LVIN and LVIN-KCγ-d connectivity matrices.

C. Left, receptive field sizes of direct VPNs are approximated by counting the number of ommatidial columns contained within the estimated receptive field edges. Receptive field sizes are plotted against the sum of synapses to KCγ-d's to show that VPNs with larger receptive fields also have stronger connectivity onto the KCγ-d population. Right, receptive field size of indirect VPNs is plotted against the sum of synapses to LVINs.

D. Left, each colored circle represents the centroid of a direct VPN receptive field (colors reflect source of visual input as shown in legend, top left). Size of the colored circle is proportional to the sum of synapses the VPN makes to the KCγ-d population. Right, each colored circle represents the centroid of an indirect VPN receptive field. Size of the colored circle is proportional to the sum of synapses to the LVIN population.

E. Effective receptive fields of five representative KCγ-d's obtained from a linear combination of their VPN inputs (direct inputs are shown in the left columns, indirect inputs are shown in the right columns). Color indicates source input neuropil and shading indicates the strength of connectivity (sum of synapses) onto the KCγ-d population (for indirect VPNs, this is obtained by multiplying VPN-LVIN and LVIN-KCγ-d connectivity matrices). Solid black, solid gray, and dashed borders differentiate VPNs that form only direct synapses with KCγ-d, VPNs that form only indirect connections to KCγ-d's through LVINs, and VPNs that form both direct and indirect connections to KCγ-d's.

Data in this figure examine the receptive field properties of VPNs with processes in the left optic lobe only.

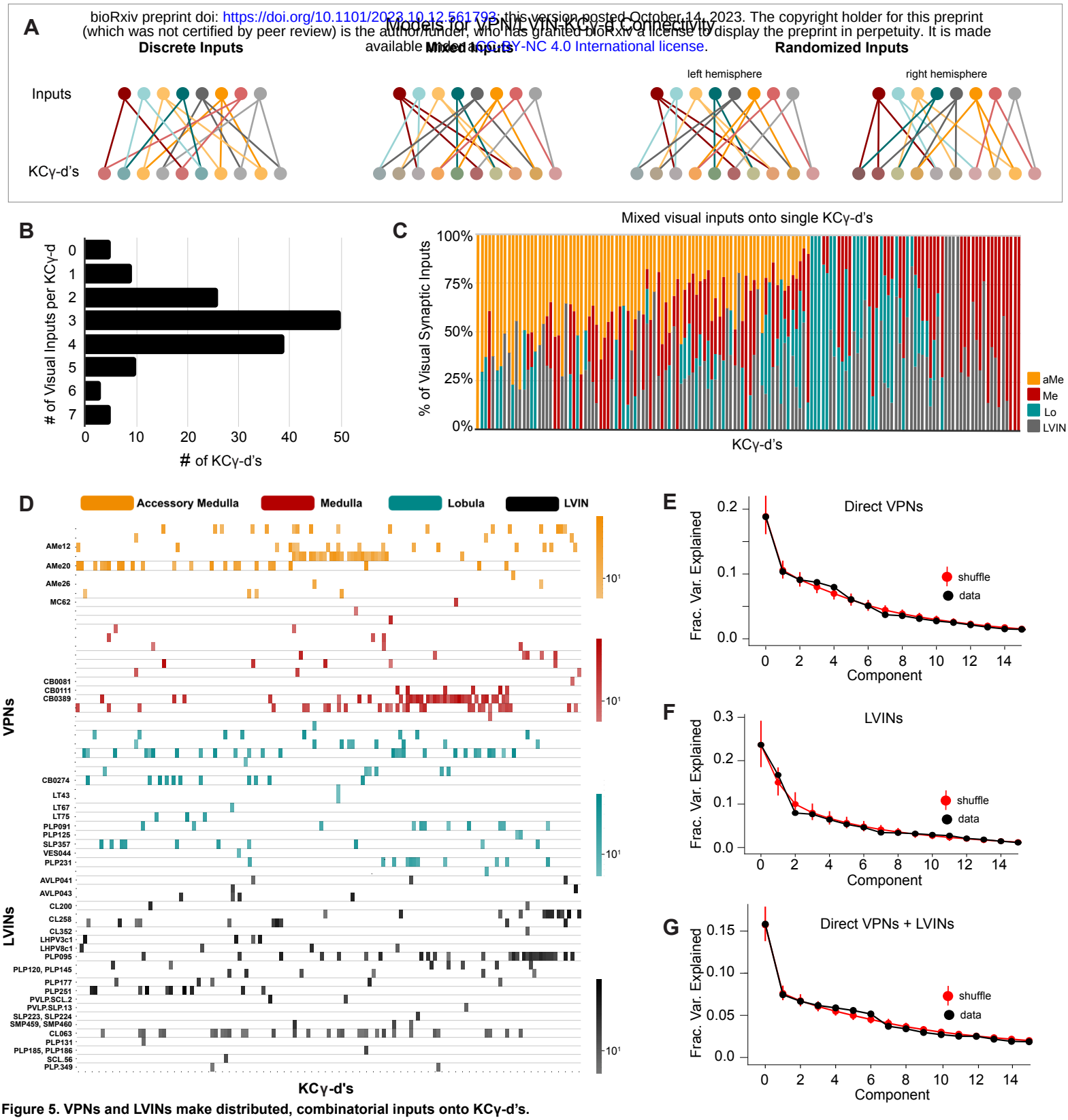

Figure 5. VPNs and LVINs make distributed, combinatorial inputs onto KCγ-d's.

A. Models illustrating potential configurations of connectivity patterns between VPNs/LVINs and KCγ-d's. Left, discrete visual channels, an example of which is organized by optic lobe neuropil origin; Middle, mixtures of visual inputs onto KCγ-d's; Right, Non-stereotyped mixtures of visual inputs onto KCγ-d's, which can only be examined across hemispheres. Note that the statistical tests we used (see Methods) to ascertain the presence of structured input onto KCγ-d's are sensitive enough to detect multiple types of structure, not only that which is illustrated on the left.

B. Individual KCγ-d's (n=147) receive 0-7 unique inputs from VPNs/LVINs. The median KCγ-d receives 3 inputs. The 5 KCγ-d's that receive 0 inputs receive inputs from olfactory projection neurons.

C. Individual KCγ-d's receive mixtures of inputs from various optic lobe or LVIN sources. Columns are the synaptic input compositions of individual KCγ-d's (n=142, i.e. the ones which receive visual input).

D. Connectivity from direct VPNs and LVINs onto KCγ-d's. VPNs are sorted by input neuropil and morphological type. LVINs are sorted by neurotransmitter and morphological type. KCγ-d's were sorted using spectral clustering (see Methods).

E. Principal components analysis of direct VPN to KCγ-d connectivity. Red circles and bars represent mean and 95% confidence intervals for variance explained by the principal components of shuffled connectivity matrices. Top PC components do not account for higher proportions of variance than shuffled matrices preserving VPN connection probability and number of inputs to each KC.

F. Principal components analysis of LVIN to KCγ-d connectivity. Red circles and bars represent mean and 95% confidence intervals for variance explained by the principal components of shuffled connectivity matrices. Top PC components do not account for higher proportions of variance than shuffled matrices preserving LVIN connection probability and number of inputs to each KC.

G. Principal components analysis of direct VPNs and LVINs to KCγ-d connectivity. Red circles and bars represent mean and 95% confidence intervals for variance explained by the principal components of shuffled connectivity matrices. Top PC components do not account for higher proportions of variance when compared to shuffled matrices preserving VPN and LVIN connection probabilities and number of inputs to each KC.

Data in this figure examine connectivity in the left hemisphere, using a ≥5 synapse threshold.

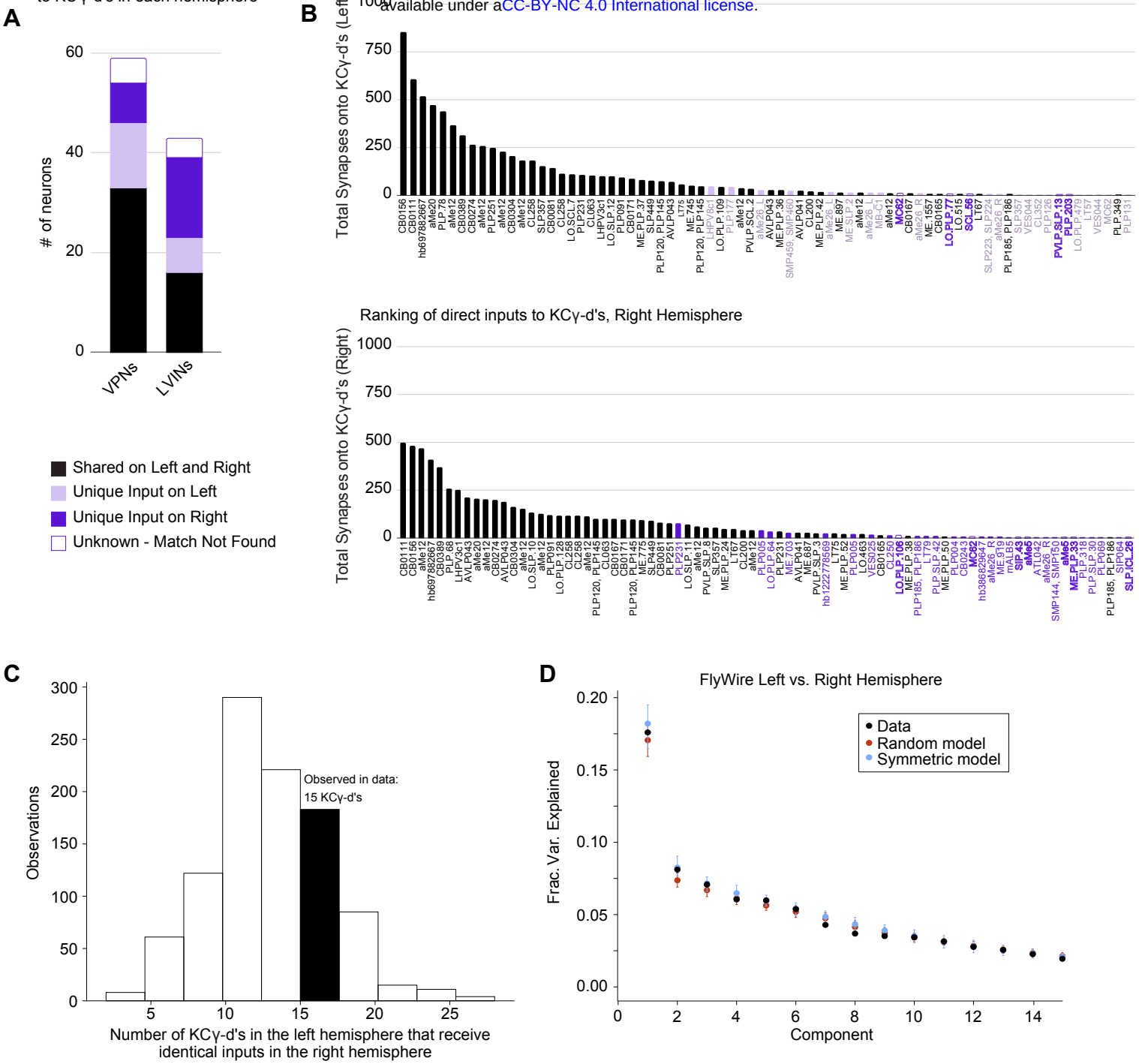

Figure 6. KCγ-d's receive a random set of inputs from VPNs and LVINs.

A. A subset of VPN and LVIN inputs in the left hemisphere (black) have a mirror copy in the opposing hemisphere that synapses with KCγ-d (n=33 VPNs, 16 LVINs). Some VPNs and LVINs are unique inputs to either the left (light purple; n= 13 VPNs, 7 LVINs) or right hemisphere (dark purple; n= 8 VPNs, 16 LVINs). For a few neurons, no mirror copy could be easily identified (white box, purple outline; n=5 VPNs, 4 LVINs).

B. Ranking of inputs to KCγ-d in left (top) and right (bottom) hemispheres. Neuron names across the x-axis are colored as in (A). The strongest inputs to KCγ-d are shared across hemispheres, while neurons unique to either hemisphere are generally found in the bottom half of inputs.

C. Histogram shows the number of KCγ-d's in the left hemisphere that receive identical VPN/LVIN input patterns in the right hemisphere for 1000 randomly shuffled VPN/LVIN to KCγ-d matrices. VPN and LVIN connection probabilities as well as the number of inputs received by each KCγ-d were preserved to match the data. In the FlyWire dataset, 15 KCγ-d's in the left hemisphere receive identical VPN/LVIN input patterns in the right hemisphere (black bar).

D. Principal components analysis on the combined left and right hemisphere VPN/LVIN to KCγ-d connectivity matrix (black). Red circles and bars represent mean and 95% confidence intervals for the variance explained by principal components of a random model in which the connectivity matrix was shuffled, preserving VPN/LVIN connection probabilities and number of inputs to each KC (1000 shuffles). Blue circles and bars represent mean and 95% confidence intervals for the variance explained by principal components of a bilaterally symmetric model in which the connectivity matrix was random but identical for each hemisphere (1000 shuffles).

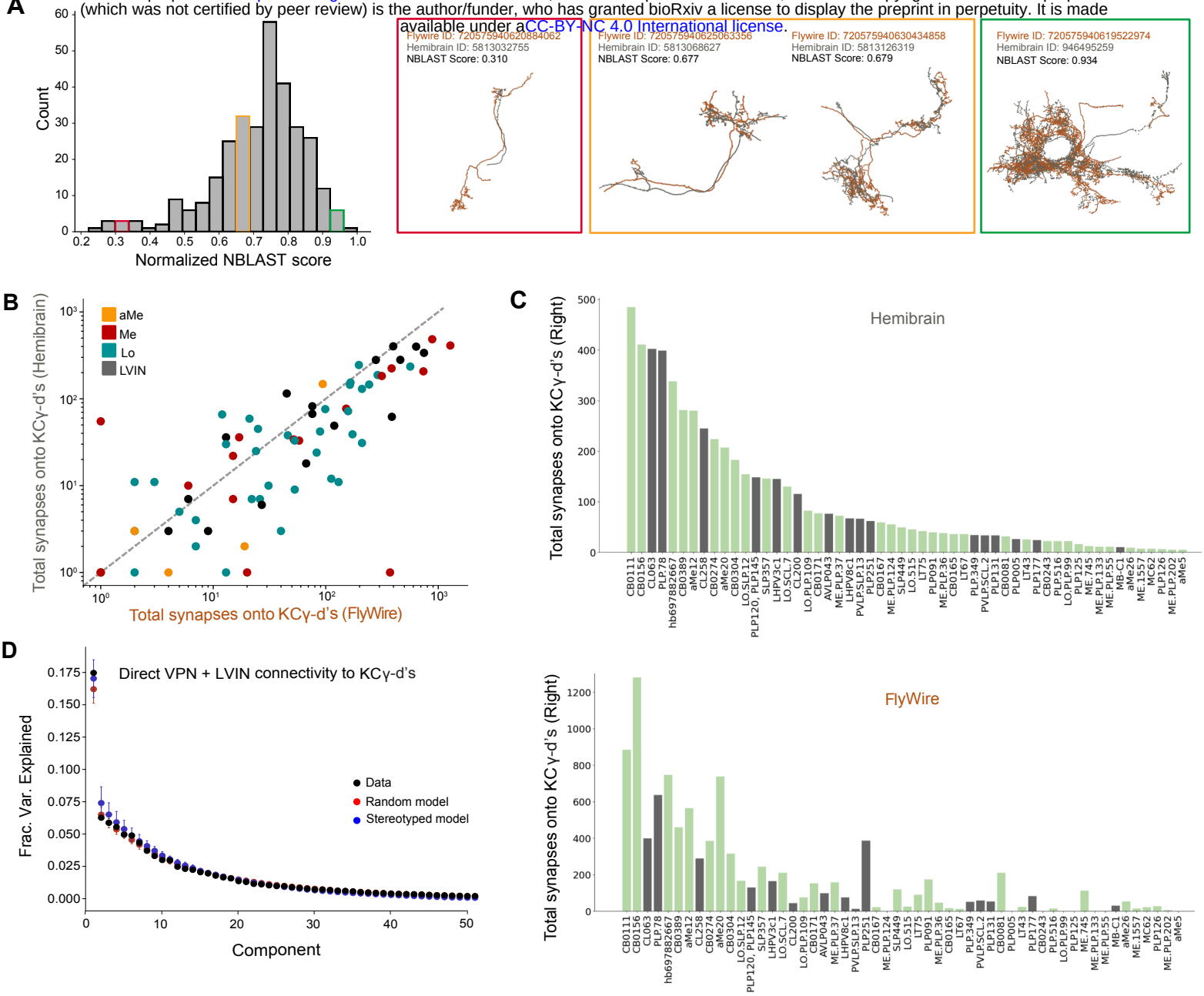

Figure 7. Prominent visual inputs to KCγ-d are shared across brains.

A. Left, distribution of NBLAST scores (normalized) when matching each FlyWire VPN or LVIN in one hemisphere to the full hemibrain dataset (see Methods). Right, representative examples of matched neurons with scores in three different NBLAST score ranges. Orange, FlyWire neuron skeleton. Gray, Hemibrain neuron skeleton.

B. For each VPN and LVIN in the Flywire dataset, the sum of synapses onto KCγ-d's in FlyWire (x-axis) are plotted against the sum of synapses its match makes onto hemibrain (y-axis). Neurons which have higher connectivity onto KCγ-d's in hemibrain also tend to have higher connectivity onto KCγ-d's in FlyWire.

C. Top, matched neurons in hemibrain are ranked by the sum of synapses made onto the KCγ-d population. Bottom, the sum of synapses onto the KCγ-d population for the FlyWire neuron matches to the hemibrain neurons in the top panel; the order is consistent with the top panel to highlight that neurons which have larger weights are largely common between the two brains. In total FlyWire neurons tend to make more synapses onto KCγ-d's, and this is likely because there are more KCγ-d's in the FlyWire brain than in the hemibrain (148 vs. 99 KCγ-d's, right hemisphere)[47].

D. Principal components analysis on VPN/LVIN connectivity to KCγ-d's (black) aggregated over both connectomes. Red circles and bars represent mean and 95% confidence intervals for the variance explained by principal components of shuffled connectivity matrices preserving VPN/LVIN connection probabilities and number of inputs to each KC. Blue circles and bars represent mean and 95% confidence intervals for the variance explained by principal components of bilaterally symmetric connectivity matrices in which VPN/LVIN-KC connectivity is random but identical in both connectomes.

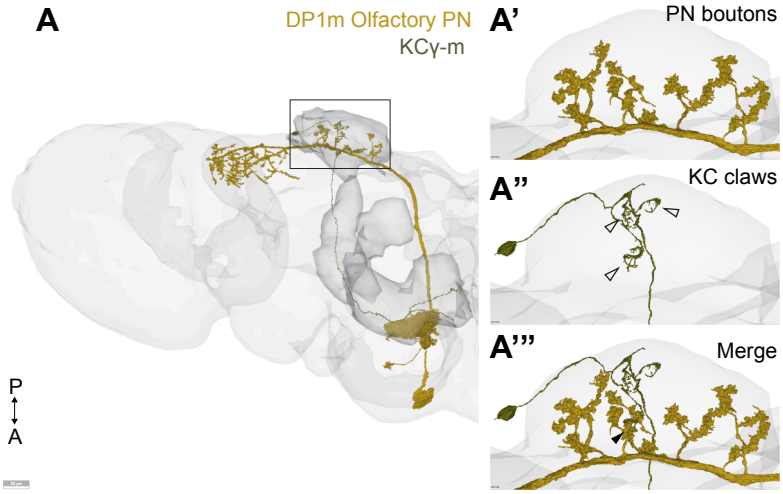

Visual PNs and KCs form bouton-claw and *en passant* synapses

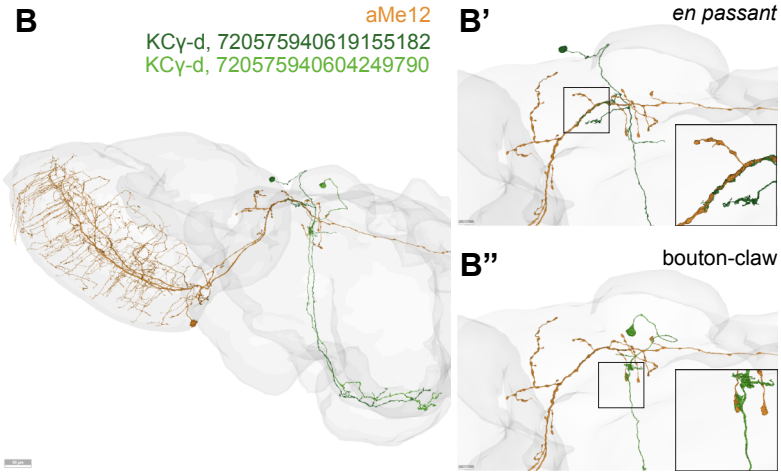

LVINs and KCs form bouton-claw and *en passant* synapses

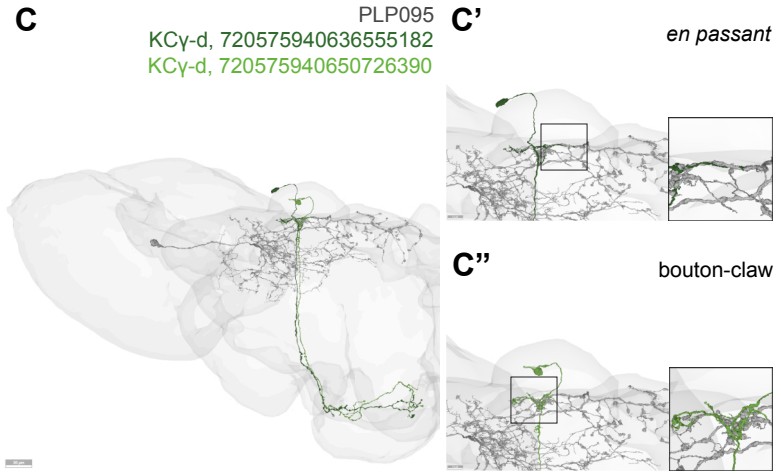

Figure 1 Supplement 1. KCγ-d's form putative bouton-claw synapses and *en passant* synapses with VPNs and LVINs.

A. Olfactory projection neurons and olfactory Kenyon cells form bouton-claw synapses that are typical of the olfactory calyx. (A') Zoom in of the mushroom body calyx, showing PN boutons. (A") KCγ-m cell with dendritic claws indicated with open arrowheads. (A"') Merge of A' and A" with bouton-claw contacts indicated by arrowheads. Scale bar for A, 20µm. Scale bar for A'-A"', 2µm.

B. Example of a VPN, aMe12, that form putative en passant synapses with one KCγ-d (B') and a putative bouton-claw synapse with another KCγ-d (B"). Insets show a zoomed in view of the boxed regions. Scale bar for A, 20µm. Scale bar for B'-B", 7.5µm.

C. Example of an LVIN, PLP095, that forms putative en passant synapses with one KCγ-d (C') and a putative bouton-claw synapse with another KCγ-d (C"). Scale bar for A, 20µm. Scale bar for C'-C", 7.5µm.

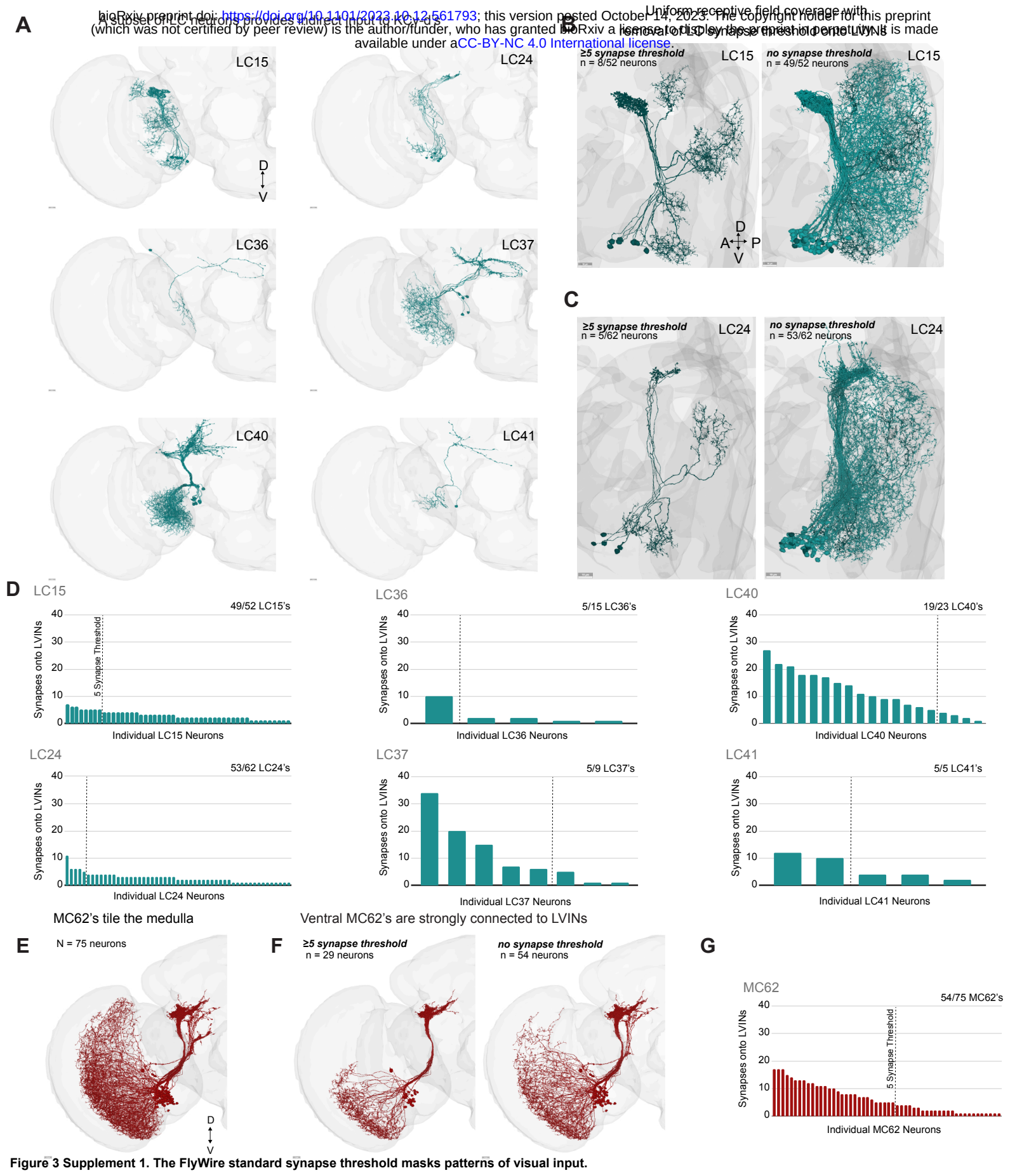

Figure 3 Supplement 1. The FlyWire standard synapse threshold masks patterns of visual input.

A. A subset of lobula columnar neurons (LCs) provide indirect inputs to KCγ-d's via LVINs. Scale bars, 10µm.

B. Left, 8/52 LC15 neurons form ≥5 synapses with LVINs, creating a sporadically filled receptive field. Right, when the synapse threshold is removed, 49/52 LC15's are now found to synapse with LVINs, creating a uniform coverage of the receptive field. Scale bars, 10µm.

C. Left, 5/62 LC24 neurons form ≥5 synapses with LVINs. Right, when the synapse threshold is removed, 53/62 LC24's are now found to synapse with LVINs. Scale bars, 10µm.

D. Number of synapses made by individual unique LC neurons onto LVINs. Dashed lines indicate the 5-synapse threshold. The fraction of total LCs that make at least one synapse with an LVIN is indicated in the upper right of each graph.

E. The population of 75 MC62 neurons annotated in FlyWire have dendrites that tile the entire medulla. Scale bar, 10µm.

F. Left, 29/75 MC62 neurons synapse with LVINs when using a ≥5 synapse threshold. These neurons cover the ventral half of the medulla. Right, when the synapse threshold is removed 54/75 MC62's are now found to synapse with LVINs but coverage is lacking in the dorsal-most region of the medulla. Scale bars, 10µm.

G. Number of synapses made by individual unique MC62 neurons onto LVINs. Dashed line indicates the 5-synapse threshold. The fraction of total MC62s that make at least one synapse with an LVIN is indicated in the upper right of the graph.

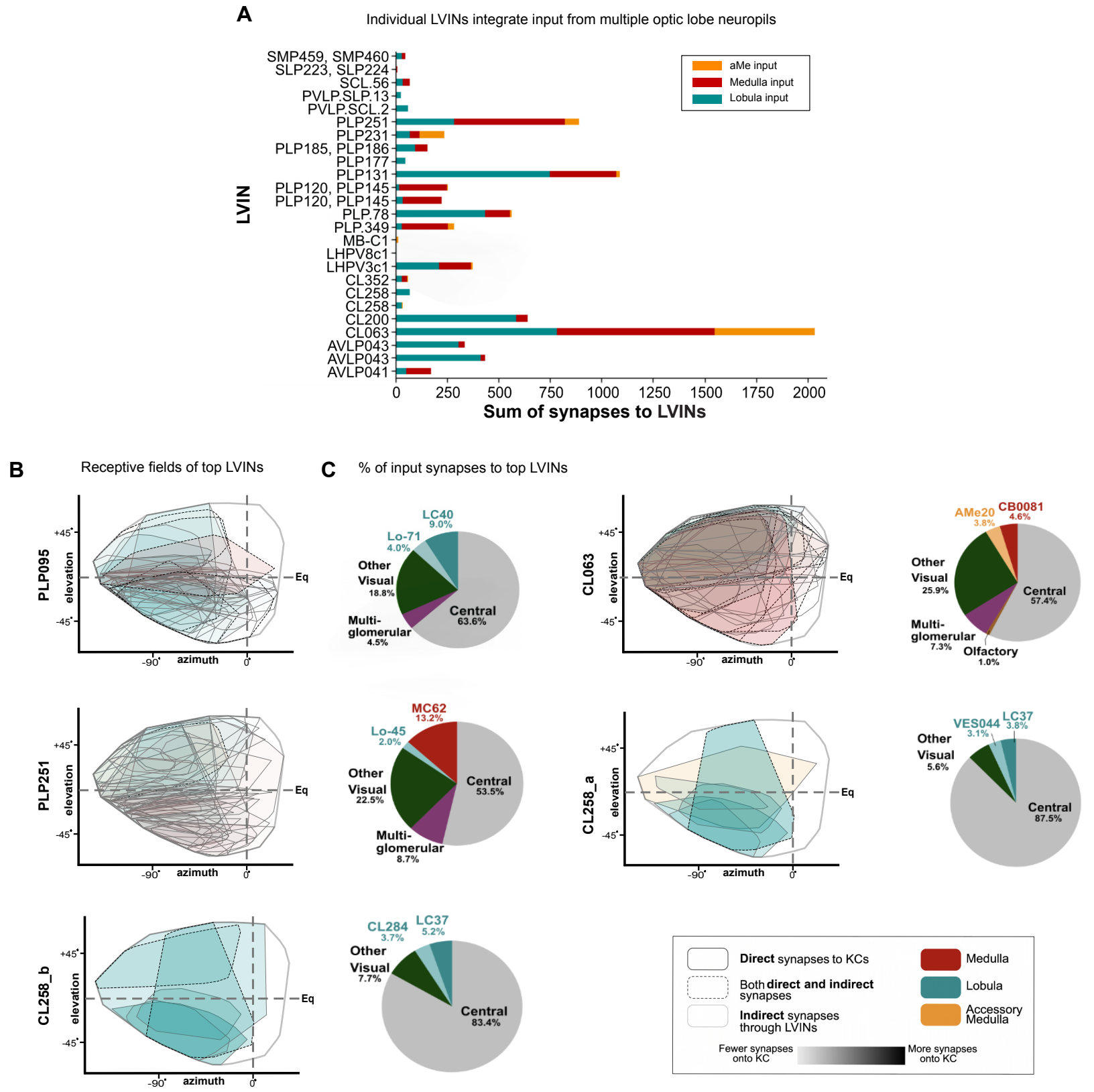

Figure 3 Supplement 2. LVINs integrate diverse sets of inputs.

A. Proportion of synapses from the primary sources of optic lobe input (aMe, medulla, and lobula) onto each individual LVIN. Most LVINs integrate a combination of input from different optic lobe neuropils.

B. The effective receptive fields of the top 5 LVINs (selected by considering the sum of synapses onto KCγ-d's) are a combination of individual input VPN receptive fields. Color indicates source input neuropil and shading indicates the strength of connectivity (sum of synapses) onto the LVIN. LVINs receive multiple visual inputs with distributed weights.

C. Percentages of direct synaptic input received from the top two input VPN classes as well as all other visual inputs to the top 5 LVINs shown in (B). Also shown are the percentages of direct synaptic input from other sensory origins (multi-glomerular, olfactory) and the central brain.

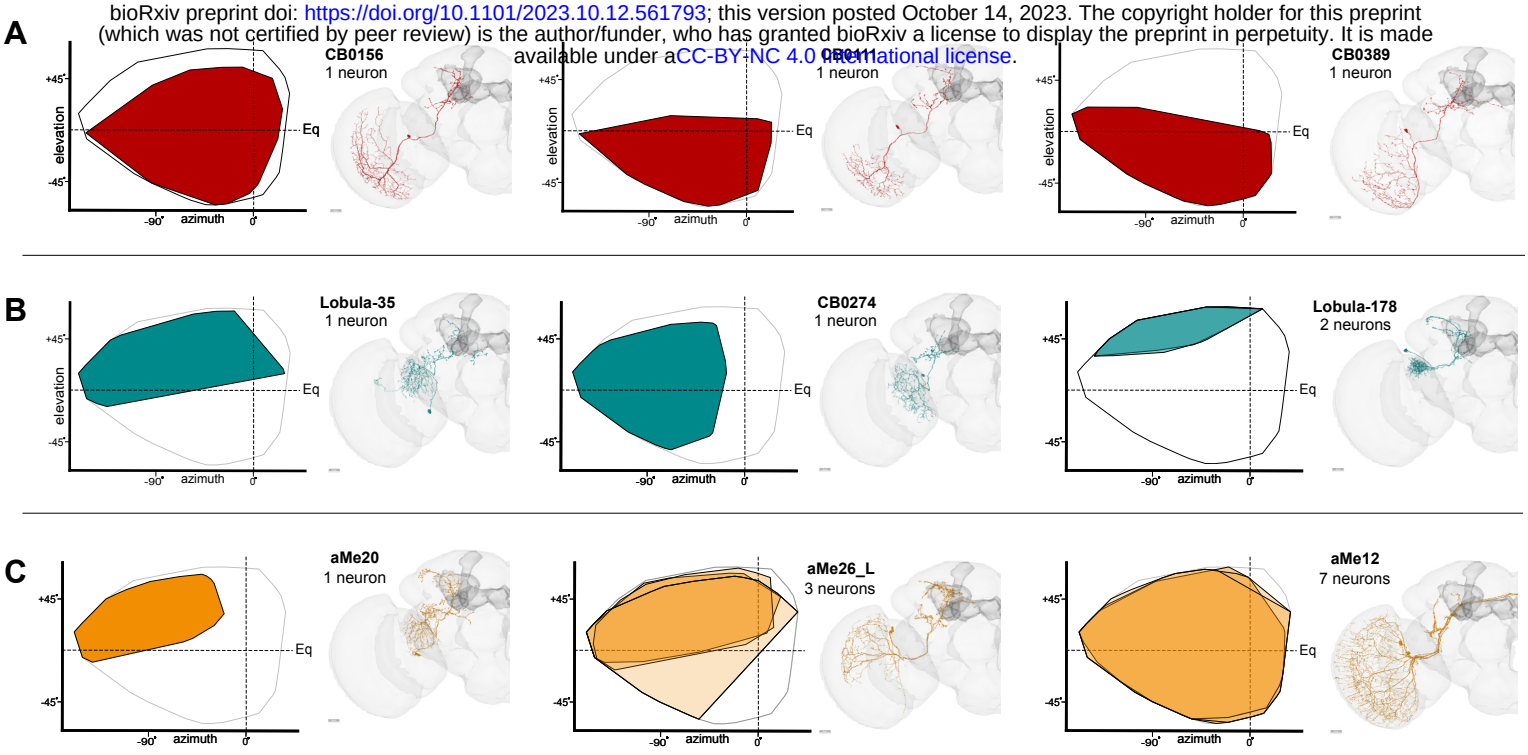

Figure 4. Supplement 1. Receptive fields of top morphological classes that contact KCγ-d's.

A. Estimated receptive fields (Mollweide projections of ommatidial viewing angles) of the top three VPN input classes that carry visual information from the medulla to KCγ-d's. For each morphological class, the receptive fields of individual neurons are overlaid, and shading indicates what proportion of the class's total synaptic input to the KCγ-d population is accounted for by that neuron.

B. Estimated receptive fields as in (A) of the top three VPN input classes that carry visual information from the lobula to KCγ-d's.

C. Estimated receptive fields as in (A) of the top three VPN input classes that carry visual information from the accessory medulla to KCγ-d's.

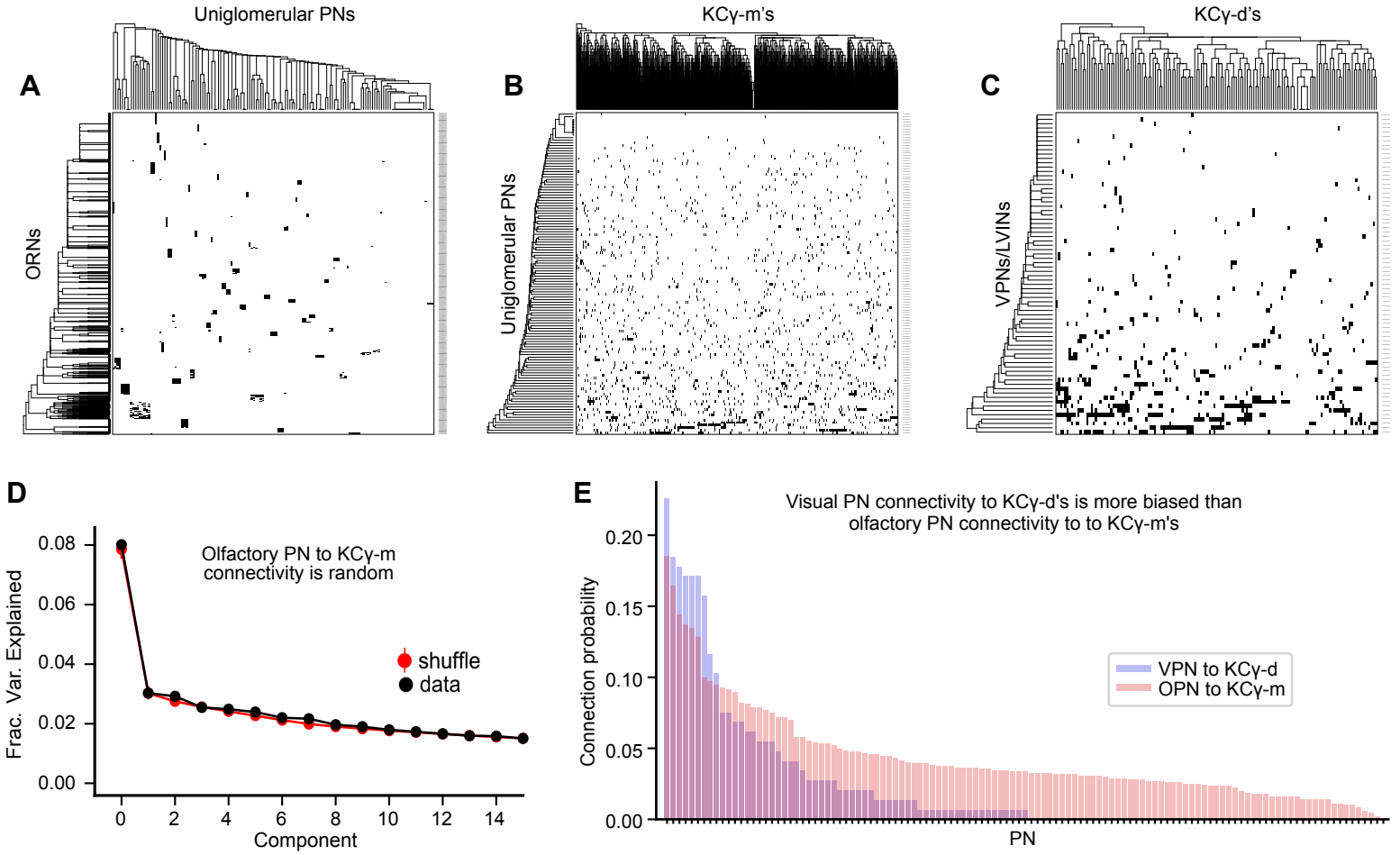

Figure 5 Supplement 1. Olfactory and visual PNs display analogous patterns of connectivity with Kenyon cells.

A. Olfactory receptor neurons (ORNs, rows) make largely discrete connections with uniglomerular olfactory projection neurons (PNs, columns). Connections were binarized using a 5 synapse threshold. Black cells indicate contacts ≥5 synapses. Rows and columns are hierarchically clustered based on partner similarity.

B. Heatmap showing binarized Uniglomerular PN-KCγ-m synaptic contacts. PNs make distributed inputs onto KCγ-d's.

C. Heatmap showing binarized VPN/LVIN-KCγ-d synaptic contacts. VPN and LVIN inputs onto KCγ-d's have a connectivity structure that is qualitatively similar to olfactory PNs and KCγ-m.

D. Principal components analysis of uniglomerular olfactory projection neuron to KCγ-m connectivity. Red circles and bars represent mean and 95% confidence intervals for variance explained by the principal components of shuffled connectivity matrices. Top PC components do not account for higher proportions of variance when compared to shuffled matrices preserving ORN connection probability and number of inputs to each KCγ-m.

E. The sorted connection probabilities of individual VPNs onto the KCγ-d population (blue) compared to the sorted connection probabilities of individual ORNs onto the KCγ-m population (red). The top VPNs have higher, biased connection probabilities onto the KCγ-d population when compared to the top ORNs connecting to the KCγ-m population.

Data in this figure examine connectivity in the left hemisphere, using a ≥5 synapse threshold.